ACCEPTED BY: *The Astronomical Journal*
Preprint typeset using LaTeX style emulateapj v. 08/13/06

arXiv:1002.3323v1 [astro-ph.CO] 17 Feb 2010

HIERARCHICAL STRUCTURE FORMATION AND MODES OF STAR FORMATION IN HICKSON COMPACT GROUP 31*

S. C. Gallagher,[1,2] P. R. Durrell,[3] D. M. Elmegreen,[4] R. Chandar,[5] J. English,[6] J. C. Charlton,[7] C. Gronwall,[7] J. Young,[7] P. Tzanavaris,[8,9] K. E. Johnson,[10,11] C. Mendes de Oliveira,[12] B. Whitmore,[13] A. E. Hornschemeier,[8] Aparna Maybhate[13] & Ann Zabludoff[14]

accepted by: The Astronomical Journal

ABSTRACT

The handful of low-mass, late-type galaxies that comprise Hickson Compact Group 31 is in the midst of complex, ongoing gravitational interactions, evocative of the process of hierarchical structure formation at higher redshifts. With sensitive, multicolor *Hubble Space Telescope* imaging, we characterize the large population of < 10 Myr old star clusters that suffuse the system. From the colors and luminosities of the young star clusters, we find that the galaxies in HCG 31 follow the same universal scaling relations as actively star-forming galaxies in the local Universe despite the unusual compact group environment. Furthermore, the specific frequency of the globular cluster system is consistent with the low end of galaxies of comparable masses locally. This, combined with the large mass of neutral hydrogen and tight constraints on the amount of intragroup light, indicate that the group is undergoing its first epoch of interaction-induced star formation. In both the main galaxies and the tidal-dwarf candidate, F, stellar complexes, which are sensitive to the magnitude of disk turbulence, have both sizes and masses more characteristic of $z = 1$–2 galaxies. After subtracting the light from compact sources, we find no evidence for an underlying old stellar population in F – it appears to be a truly new structure. The low velocity dispersion of the system components, available reservoir of H I, and current star formation rate of $\sim$10 $M_\odot$ yr^{-1}, indicate that HCG 31 is likely to both exhaust its cold gas supply and merge within ~ 1 Gyr. We conclude that the end product will be an isolated, X-ray-faint, low-mass elliptical.

Subject headings: galaxies: star clusters — galaxies: interactions — galaxies: evolution — galaxies: clusters: individual (HCG 31)

1. INTRODUCTION

Massive elliptical galaxies are preferentially found in high density environments such as galaxy clusters – galaxy morphology and environment are clearly coupled in the local Universe (Dressler 1980). However, the mechanism for morphological transformation from star-forming and disk-dominated to quiescent and bulge-dominated is still uncertain. For example, is ram-pressure stripping important as a galaxy plows through the hot intracluster medium (ICM)? Alternatively, gravitational interactions from harassment to mergers might dominate the transformation process. Secular evolution whereby gas is sheparded inwards, thus triggering star formation and exhausting the material for subsequent generations of stars, could be important. The action of an active galactic nucleus (AGN) may also significantly alter its host in dense regions.

Furthermore, the question of *when* morphological transformation occurs in the hierarchical build-up of a galaxy cluster from subunits of galaxy groups is still open. Already, the demographics of cluster galaxies as a function of redshift indicate that some galaxy evolution occurs prior to cluster infall (e.g., Dressler et al. 1997). Determining if galaxies are *primarily* processed while still contained within the unit of the group will shed light on the influence of the ICM (e.g., Zabludoff et al. 1996; Zabludoff & Mulchaey 1998, 2000). Studies of compact group galaxies offer the promise to further elucidate this issue, as in their cores they have the same galaxy number densities as galaxy clusters, but without (with a few exceptions) an X-ray emitting intragroup medium (IGM). The lower velocity dispersions ($\sigma \sim 10^2$ km s^{-1}) in groups compared to clusters ($\sigma \sim 10^3$ km s^{-1}) also prolong gravitational interactions. This context is relevant therefore for evaluating the role of gravitational interactions in morphological transformation before the cluster potential or ICM becomes dominant.

Recent *Spitzer* results on compact group galaxies sug-

* Based on observations made with the NASA/ESA Hubble Space Telescope.
[1] Department of Physics & Astronomy, The University of Western Ontario, London, ON, N6A 3K7, CANADA; *sgalla4@uwo.ca*
[2] Department of Physics & Astronomy, University of California – Los Angeles, Los Angeles CA, 90095–1547
[3] Department of Physics & Astronomy, Youngstown State University, Youngstown, OH 44555
[4] Department of Physics & Astronomy, Vassar College, Poughkeepsie, NY 12604
[5] Department of Physics & Astronomy,University of Toledo, Toledo, OH 43606-3390
[6] Department of Physics & Astronomy, University of Manitoba, Winnipeg, MN, R3T 2N2, CANADA
[7] Department of Astronomy and Astrophysics, The Pennsylvania State University, University Park, PA 16802
[8] Laboratory for X-ray Astrophysics, NASA's Goddard Space Flight Center, Greenbelt, MD 20771
[9] Department of Physics and Astronomy, The Johns Hopkins University, Baltimore, MD 21218
[10] Department of Astronomy, University of Virginia, Charlottesville, VA 22904-4325
[11] National Radio Astronomy Observatory, Charlottesville, VA 22903-2475
[12] Instituto de Astronomia, Geofísica, e Ciências Atmosféricas da Universidade de São Paulo, São Paulo, Brazil
[13] Space Telescope Science Institute, Baltimore, MD 21218-2463
[14] Steward Observatory, University of Arizona, Tucson, AZ 85721

gest that the transformation from neutral gas-rich and actively star-forming galaxies to neutral gas-poor and quiescent galaxies can occur quite rapidly in this environment. Specifically, Johnson et al. (2007) found that most member galaxies in compact groups in an early evolutionary state (defined by a high ratio of their H I to dynamical masses) are actively star-forming as judged from their infrared luminosities and colors, while those with little H I are dominated by the stellar photospheric emission of old stellar populations. While this is perhaps not surprising, there is a notable gap in the distribution of infrared spectral indices of the compact group population compared to a sample of local galaxies matched in optical luminosity from the SINGS sample (Kennicutt et al. 2003); the SINGS galaxies have a continuous distribution of infrared properties (Gallagher et al. 2008). The lack of compact group galaxies in the intermediate region of infrared color-space suggests that this location is crossed quickly (Johnson et al. 2007; Walker et al. 2009). This picture of galaxy processing in this environment is further demonstrated by the H I deficiency of late-type compact group galaxies relative to those in loose groups and the field (Williams & Rood 1987; Verdes-Montenegro et al. 2001).

Local Hickson Compact Groups (HCGs; Hickson 1993) are therefore promising testbeds for investigating morphological galaxy transformations nearby that are directly relevant to galaxy evolution from 'blue cloud' to 'red sequence' in the color-absolute magnitude plane (e.g., Hogg et al. 2004; Balogh et al. 2004; Willmer et al. 2006). In currently dense environments (i.e, galaxy clusters), this change likely occurred at $z = 1$–2 (e.g., Cucciati et al. 2006; Franzetti et al. 2007; Cooper et al. 2007). Of the nearest HCGs, HCG 31 (NGC 1741) is perhaps the best example of catching this process in progress. This system is comprised entirely of low mass (1–8×10^9 $M_\odot$; Verdes-Montenegro et al. 2005), late-type galaxies in a compact ($\sim 1.4'$ [~ 23 kpc] diameter) configuration. It is clear from the multicolor image in Figure 1 that each of galaxies in the group is disturbed, and tidal tails, bridges, and dwarfs are prominent.

In this paper, we present deep, three band *HST* ACS images of HCG 31, using high angular resolution and sensitivity to probe modes of star formation from the star cluster (∼pc) to star complex and dwarf galaxy (∼kpc) scale. Our goal is to investigate hierarchical structure formation through an in-depth study of this system. In particular, we want to study the mechanism by which neutral gas is consumed in dense and dynamically young environments.

1.1. *Studies of HCG 31 to Date*

From visual inspection of Figure 1, the primary galaxies that comprise HCG 31 (A+C, B, and G) are clearly disturbed, and the presence of bright tidal structures (E, F, and H) further supports the importance of gravitational interactions in the recent history of the system. An additional galaxy, Q to the north, is shown to be part of the group based on radial velocity (Rubin et al. 1990) and H I structure (Verdes-Montenegro et al. 2005) that link it to other group members. UV, optical, and infrared photometry of A+C indicate active recent and ongoing star formation (e.g., Iglesias-Paramo & Vilchez 1997; Johnson et al. 1999; Johnson & Conti 2000; Johnson et al. 2007). This conclusion is supported by spectroscopic detections of Wolf-Rayet signatures in A+C and F (Kunth & Schild 1986; Rubin et al. 1990; Conti 1991; López-Sánchez et al. 2004).

The high levels of star formation and irregular morphology of the A+C complex imply a recent starburst triggered by their mutual interaction. Further study of the H I morphology and velocity field of the entire system indicates that not just one but multiple interactions have led to the current configuration (e.g., Amram et al. 2004; Mendes de Oliveira et al. 2006). Notably, much of the neutral hydrogen in the group has been removed from the galaxies (Verdes-Montenegro et al. 2001) yet remains bound to the group in tidal structures; 60% percent of the H I is located in four tidal tails and one bridge linking six of the member galaxies (Verdes-Montenegro et al. 2005). In sum, though the group as a whole is not H I deficient, the *individual galaxies* are (Verdes-Montenegro et al. 2001).

While Rubin et al. (1990) conjectured that HCG 31 will coalesce into a single large elliptical in only a few orbital periods, this is still an open issue. Specifically, will HCG 31 transition in the near term (within ~ 1 Gyr) into an evolved state such as a 'fossil group' – a single, elliptical galaxy with a bright X-ray halo (Jones et al. 2003)? As HCG 31 is one of the most compact groups in the Hickson et al. (1992) Atlas with most of the H I stripped from its individual galaxies, it is perhaps the most likely late-stage merger candidate (Williams et al. 1991).

Can the modes of star formation — from the populations of parsec-scale star clusters to kpc-scale star-forming complexes and dwarf galaxies — in this compact galaxy group elucidate the mechanism of galaxy transformation in the high redshift universe? With our new ACS imaging as well as IR+UV constraints on the current star formation rates (SFRs) throughout the system, we aim to shed new light on the current state of star formation in HCG 31 as well as its future evolution.

At the H I redshift, $z = 0.01347 \pm 0.00002$ (Meyer et al. 2004), of HCG 31, its distance is 58.3 Mpc (yielding a distance modulus, DM =33.83) and $1''$ corresponds to 275 pc ($\Omega_{\rm M} = 0.3$; $\Omega_\Lambda = 0.7$; $h_{100} = 0.7$; Spergel et al. 2007). Using a Galactic $E(B-V) = 0.051$ (Schlegel et al. 1998), all magnitudes and colors throughout the text have been corrected for Galactic reddening.

2. OBSERVATIONS

Observations of HCG 31 were obtained with *HST* ACS/WFC using the F435W, F606W, and F814W filters. Throughout, we use B_{435}, V_{606}, and I_{814} to refer to the F435W, F606W, and F814W ACS filters and the magnitudes measured in those filters, respectively. The data were taken on August 8, 2006 with exposure times of 1710 seconds in F435W, 1230 seconds in F606W, and 1065 seconds in F814W. The observations for each filter were taken with three equal exposures, using a three-point dither pattern. The implementation of `MultiDrizzle`[16] in the *HST*/ACS data pipeline provides combined, geometrically corrected, and cosmic ray

[16] `MultiDrizzle` is a product of the Space Telescope Science Institute, which is operated by AURA for NASA. See http://stsdas.stsci.edu/pydrizzle/multidrizzle.

cleaned images. For the analysis of point sources, we used the standard *HST* pipeline products with a nominal pixel scale of 0.″05 per pixel. For analysis of the extended sources, we ran `MultiDrizzle` with the pixel scale set to 0.″03 per pixel to improve the spatial resolution.

In addition to the new *HST* observations that are the primary focus of this paper, we also present new *Swift* and *GALEX* observations of HCG 31, and incorporate the *Spitzer* IRAC and MIPS images presented in Johnson et al. (2007). This is part of a long-term, in-depth multiwavelength investigation into a sample of 12 HCGs using the combination of *HST* three-color imaging (six complete), *Chandra* ACIS imaging spectroscopy (eight total as part of archival and new observations), *Spitzer* IRAC and MIPS imaging (already in hand; Johnson et al. 2007), and *Swift* Ultraviolet Optical Telescope (UVOT) and *GALEX* multifilter imaging (Tzanavaris et al., in prep.).

For the purposes of associating star-forming structures within the individual features in HCG 31, we have defined polygonal boundaries for the galaxies and tidal regions as marked on the three-color ACS image shown in Figure 2.

2.1. *Star Cluster (SC) Candidate Identification and Photometry*

At the redshift distance of HCG 31 of 58.3 Mpc, star clusters are expected to be unresolved or marginally resolved with a 0.″05 ACS pixel corresponding to 13.8 pc. Therefore, as a first step to finding star cluster candidates, the entire ACS field was searched for point sources.

Point-source photometry was performed on the pipeline-drizzled images using the point source function (PSF) fitting algorithm of Stetson (1987) as implemented in IRAF.[17] Given that the V_{606} image was the deepest of the three, it was the primary one used for point-source identification and filtering. Magnitudes are given in the Vega system using the zeropoints appropriate for August 2006:[18] 26.406, 25.767, and 25.520, for V_{606}, B_{435}, and I_{814}, respectively.

We searched for point-source candidates using the median-divided V_{606} image with a threshold of 0.25 counts; source-free background regions have standard deviations of ~ 0.07 counts. The weight-map image from the pipeline processing was used to filter the candidate list to remove artifacts from chip edges and the diffraction spikes from saturated stars; point source candidates were rejected if their weight map values were less than the median minus twice the standard deviation of the distribution. Visual inspection confirmed that this method effectively screened out spurious detections without discarding real point sources.

PSF models in each filter were constructed from the brightest, isolated, and unsaturated stars. Their radial profiles were checked for irregularities, and 13, 13, and 18 PSF stars were used in V_{606}, B_{435}, and I_{814}, respectively. Moffat functions were used to fit the PSF in each case, with a constant PSF in V_{606}, and linearly variable PSFs for B_{435} and I_{814}. The `daophot` photometry was compared to aperture photometry for the PSF stars within a 0.″5 (10 pix)-radius circular aperture in order to determine the aperture correction. To these values, the aperture correction from 0.″5 to infinity from Sirianni et al. (2005) was added. Finally, the photometry was corrected for Galactic extinctions of A_{606}=0.144, A_{435}=0.210, and A_{814}=0.093.

For the final star cluster (SC) candidate catalog, objects were required to have $M_{V_{606}} < -9$ (to eliminate contamination from individual young stars), be detected in all three filters with magnitude error $\sigma_{\rm mag} < 0.3$ and $-2 < sharp < 2$ (*sharp* is a measure of the width of the data relative to the model psf; $sharp = 0$ indicates a width well-matched to the psf) in each and $\chi < 3$ in I_{814}. We used I_{814} for the χ criterion because the model PSF is best determined in that image. Furthermore, if SC candidates are marginally resolved because of extended, nebular Hα emission, this will not be a factor in I_{814}. (We do not want to eliminate these interesting candidates from our catalog.) Finally, color cuts of B_{435}–$V_{606} < 1.5$ and V_{606}–$I_{814} < 1.0$ were imposed to reduce contamination from foreground Galactic stars. These cuts were chosen to eliminate a distinct clump of sources in color-color space that are well-isolated and far from the expected colors of star clusters. The SC candidate numbers by region are given in Table 1, and a B_{435}–V_{606} vs. V_{606}–I_{814} plot with the sources that meet our criteria as outlined above are presented in Figure 3. To identify the youngest clusters with nebular emission, we draw a diagonal line in Figure 3 that crosses the evolutionary tracks with nebular emission at $\tau \sim 5 \times 10^6$ yr. This conservative line takes into account typical photometric errors such that all SC candidates to the left of that line have colors significantly distinct from the evolutionary tracks without nebular emission. The numbers and fractions of SC candidates with these colors for each region of HCG 31 are indicated in columns 5 and 6 of Table 1.

We imposed stricter point-source selection criteria to identify globular cluster candidates, and extend the magnitude limit to $M_{V_{606}} < -7.8$ to reach the expected peak of the globular cluster luminosity function. Following Rejkuba et al. (2005), we used a hyperbolic filter in the sharpness vs. magnitude plane and a hyperbolic filter in the magnitude error vs. magnitude plane set using the output photometry from the V_{606}-band completeness tests (see Fig. 3 in Rejkuba et al. 2005 and §2.2) to include $\sim 97\%$ of the detected artificial point sources. Point sources were also required to have $\sigma_{\rm mag} \leq 0.3$, $\chi \leq 3$, and $-2 \leq sharp \leq 2$ in all three filters. These criteria rejected a large fraction of the brightest ($M_{V_{606}} < -9$) and bluest (in V_{606}–I_{814}) point sources, indicating that many of them are marginally resolved. This is perhaps not surprising, as the wide V_{606} filter includes Hα emission, and most of these sources have colors consistent with a strong nebular contribution. The spatial scale of the Hα-emitting region surrounding a young star cluster is frequently larger than that of the stars alone. Those candidates with colors consistent with older star clusters are typically fainter and unresolved, as expected.

2.2. *Completeness*

Using `addstar` in the `daophot` package, we added 3000 artificial stars to the pipeline-drizzled V_{606} image evenly

[17] IRAF is distributed by the National Optical Astronomy Observatory, which is operated by the Association of Universities for Research in Astronomy (AURA) under cooperative agreement with the National Science Foundation.

[18] http://www.stsci.edu/hst/acs/analysis/zeropoints/

distributed between magnitudes 24 through 28 (before aperture and extinction corrections), and then ran the photometric pipeline on these data. Sources were considered detected if their input and output positions matched within 0.″075 (1.5 pix). Using the distributions of sharpness, *sharp*, vs. magnitude, and magnitude error, $\sigma_{\rm mag}$, vs. magnitude, we then set the same strict point-source selection criteria described in §2.1. Of the detected sources, these filters eliminated an additional $\sim$ 3%. From the ratio of numbers of detected point sources to input artificial stars as a function of magnitude, the V_{606} 90% and 50% complete magnitude limits were found to be 26.43 and 27.42 (including aperture and extinction corrections), respectively. For the B_{435} and I_{814} tests, the same input artificial star catalog was used as for the V_{606} image with the positions corrected for the image offsets. The V_{606} detected objects were then run through the B_{435} and I_{814} photometric pipelines. Objects were filtered using only the constant absolute $\sigma_{\rm mag}$, χ, and *sharp* limits defined above, which eliminated $1-2$% of the sources. The subsequent B_{435}/I_{814} 90% and 50% completeness limits were 26.73/26.51 and 27.33/27.18, respectively. Given the different aperture and extinction corrections in each filter, the input artificial star catalog had effective colors of B_{435}–V_{606}= -0.13 and V_{606}–I_{814}= 0.04.

Given that most of the young SC candidates are located within the group galaxies, we also determined the completeness limits within A+C and B, with boundaries corresponding to the regions shown in Figure 2 where the average surface brightness and background noise are considerably higher. The 90% $V_{606}/B_{435}/I_{814}$ completeness limits are 25.02/24.96/25.10. For a distance modulus of 33.83, even these limits are significantly fainter than the apparent magnitude of 24.83 corresponding to an absolute V_{606} luminosity limit of $M_{\rm V_{606}}< -9$.

2.3. *Star-Forming Complexes*

Complexes are isolated, high surface-brightness, star-forming knots whose sizes and masses are sensitive to the velocity dispersion in the gas. Visually, they are often identified as "beads on a string" along spiral arms. Galaxy disks stirred up by tidal interactions would be expected to have larger and more massive complexes as the scale for gravitational collapse (analogous to the Jeans length, but for turbulent rather than thermal velocities) is correspondingly larger. Complexes in HCG 31 were identified from the B_{435} and composite images, visually and with the use of contour plotting, and photometered with rectangular apertures from the custom multidrizzled images (1 pix = 0.″03). For consistency with previous work in the literature (see §3.6 and §3.7), no background subtraction was done. The complexes were typically larger than $\sim$20 pixels in diameter (corresponding to $\sim$150 pc), with outer boundaries $\sim 10\sigma$ above the background. For the sake of comparison with other systems, the focus was on identifying the largest and brightest complexes (which are the most apparent both locally and at high redshift), and the sample is therefore incomplete. There were 40 such complexes: 11 each in regions A+C, B, and G, 3 in region E, and 4 in region F, as shown in Figure 4 and 5 and listed in Table 2. The complexes in Region G correspond to the "optical knots" noted in ground-based unsharp-masked B-band images by Verdes-Montenegro et al. (2005). A visual examination of ground-based g and i images (Mendes de Oliveira et al. 2006) found no complexes of comparable size or brightness in the northern galaxies Q and R outside of the ACS field of view.

The complex diameters in HCG 31 range from $\sim$150 to 875 pc. In all cases, they are significantly resolved, and while they may encompass several SC candidates, the SC candidate and complex sizes do not overlap. In nearby spirals, the sizes of the largest complexes scale with the absolute magnitude of the galaxy (Elmegreen et al. 1994, 1996) and range from $\sim$150 pc for M_B=–16 to $\sim$1500 pc for M_B = –21. The absolute V magnitude for HCG 31 A+C is –20.7 (for DM = 33.83; Conti 1991), with $M_{\rm B_{435}}$ = –20.0 based on our *HST* image; its complex diameters range from 190–540 pc. B and G are measured to have $M_{\rm B_{435}}$ of –18.5 and –18.9, with complexes ranging from 165–190 pc and 140–400 pc, respectively. These are comparable to the sizes of complexes in local spirals with similar absolute magnitudes. The complexes in the tidal debris of HCG 31 are anomalously large; region E, with $M_{\rm B_{435}}$ = –16.5, has a complex with a diameter of 875 pc, and region F, with $M_{\rm B_{435}}$ = –15.8, has a complex of 550 pc. These values are comparable to what is observed in local Blue Compact Dwarf (BCD) galaxies and factors of 2–3$\times$ larger than those in Sm and irregular galaxies of similar magnitudes (Elmegreen et al. 2006).

2.4. *Extended Sources*

To search for extended sources that might be identified with either tidal dwarf galaxy candidates or dissolved clusters, we ran the `SExtractor` software package (Bertin & Arnouts 1996) four times, each time with a different background smoothing size, which typically favors objects of different sizes. After merging the catalogs, multiple detections were combined. The 'best' detection was chosen to be (in order) the roundest, biggest, and least stellar source. By visual inspection of the extended sources (particularly in the tidal debris of E, F, and H) identified by these means, no obvious dwarf galaxy candidates were evident. The majority of the most significant candidates can be identified either with the complexes or marginally resolved SC candidates. Furthermore, the B_{435}–V_{606} and V_{606}–I_{814} color distributions of the `SExtractor` sources were consistent with these populations. Therefore, we do not find a distinct population of extended sources to identify as either dwarf galaxy candidates or dissolved clusters.

2.5. *Evolutionary Track Models*

We used the evolutionary tracks of the Bruzual & Charlot (2003) instantaneous burst model assuming a Salpeter initial mass function (IMF), a stellar mass range from 0.1–100 $M_\odot$, and 1/5 solar metallicity, consistent with the range of $Z/Z_\odot$=0.2–0.4 found by López-Sánchez et al. (2004) for this system. The spectra at each grid point in time have been convolved with our filter set to obtain colors and magnitudes.

The Bruzual & Charlot (2003) models do not include a contribution from nebular emission. Emission lines such as Hα and [O III] can significantly affect the colors of star clusters with ages $\leq$ 10 Myr. Given that the F606W filter is quite broad, strong Hα emission at the redshift

of HCG 31 will boost the V_{606} fluxes, thereby reddening the B_{435}–V_{606} colors and making the V_{606}–I_{814} colors bluer (e.g., Vacca & Conti 1992; Conti et al. 1996). To calculate evolutionary tracks that incorporate a model of nebular emission, we used the `Starburst99`[19] (Leitherer et al. 1999) emission-line strengths for Hα and Hβ for the same IMF and metallicity burst as given above. Another strong line is [O III], which is not included in the `Starburst99` models. To estimate the maximum expected contribution of [O III] to the colors, we used the highest value of 0.7 for the ratio of log([O III]/Hβ) observed in the KISS sample of low-mass star-forming galaxies (e.g., Salzer et al. 2005); these values have been included in the calculation of the nebular tracks.

2.6. *Intrinsic Reddening*

The colors of young star clusters are often reddened by the dusty clouds in which they are born. The magnitude and direction of an A_{606}=1 Galactic reddening vector (Cardelli et al. 1989) is plotted in the color-color and color-magnitude diagrams (see Figs. 3 and 6). This may not be appropriate for these galaxies, given their lower metallicities ($Z/Z_{\odot}$ = 0.2–0.4; López-Sánchez et al. 2004), but is conservative and consistent with convention in the literature. The V_{606} filter covers strong nebular emission lines such as [O III] and Hα from the youngest star clusters at the redshift of HCG 31, and as we showed in §2.5 the inclusion of this flux stretches the predicted evolutionary tracks down and to the left in Figure 3, nicely localizing very young star clusters still surrounded by interstellar material in color-color space. The reddening vector is nearly perpendicular to the tracks including nebular emission. Therefore, as long as extinction does not push too many star clusters below our selection limit of $M_{\rm V_{606}} < -9$, the youngest clusters will still be identified as such.[20] This is not the case however, for older clusters which no longer ionize nearby interstellar gas. In this situation, shown as the solid line in the same Figure, the reddening vector is nearly parallel to the tracks themselves, making it difficult to quantitatively estimate the total extinction on a cluster by cluster basis; to do so would require U-band data of comparable resolution (e.g., Whitmore et al. 1999). The colors therefore give upper limits for age estimates.

We can get an independent assessment of extinction on larger physical scales from mid-infrared observations taken with the IRAC instrument on *Spitzer*. From the *Spitzer* IRAC images presented in Johnson et al. (2007), the strongest dust emission is present at the A+C interface. This is illustrated as the reddish-orange glow in Figure 1 (also see Fig. 4 of Johnson et al. 2007). At 8μm, Galaxy B is quite faint, and the tidal debris is largely invisible; therefore we do not expect significant dust extinction on average in those regions. The asymmetry in the disk of G is also evident in this representation. Therefore, in general we expect dust extinction will be most problematic in the main interaction region between A+C and the western star-forming ring of G.

[19] http://www.stsci.edu/science/starburst99/

[20] An assumption underlying this assertion is that ionizing stellar flux must be able to escape its natal dust cloud and still encounter sufficient gas to create detectable nebular emission.

2.7. Swift *and* GALEX *UV Imaging*

We used UV observations taken with *Swift*/UVOT and *GALEX* to probe star formation activity in HCG 31 (see Tzanavaris et al., in preparation for details). Briefly, we calculated background-subtracted fluxes at the effective wavelengths of the U, $UVW1$, $UVM2$, $UVW2$ UVOT filters (3501, 2634, 2231, 2030Å) and the NUV and FUV *GALEX* filters (2271 and 1528Å) in the galaxies and tidal structures using the Johnson et al. (2007) apertures. These values have been corrected for Galactic extinction (Schlegel et al. 1998; Cardelli et al. 1989) and are listed in Table 3. The errors include a systematic error that reflects the uncertainty in the zeropoints. No corrections for intrinsic extinction are included.

Qualitatively, we note that the significant flux levels in the *Swift* $UVW2$ and *GALEX* FUV filters are indicative of stellar populations characterized by massive stars with ages of a few Myr. This is consistent with previous UV work that only covered a small area in the central region of A+C (Conti et al. 1996). The *GALEX* NUV data has been included as purple in Figure 1, and is consistent with the *Swift* $UVM2$ emission. We combine the UV and *Spitzer* 24μm fluxes to obtain star-formation rate estimates in §3.3.

2.8. *Multicolor Images*

Given the wealth of information from the optical, infrared and ultraviolet images, we have constructed two full-field, multicolor images. The first, Figure 1, incorporates images from five bands: *GALEX* (NUV), *HST* (B_{435}, V_{606}, and I_{814}) and *Spitzer* (8 μm), and the second, Figure 2, is a three-color composite of *HST* data only. All data were converted to flux density units of erg s^{-1} cm^{-2} Å^{-1}. These values were initially distributed to the greyscale range logarithmically. The `Karma` visualization package (Gooch 1996) was used to rotate the data and regrid the non-*HST* data to the *HST* pixel scale. With this, we also further adjusted the greyscales, for example, to emphasize the brightest regions in the non-*HST* data. The remaining data manipulation was done using `GIMP`.[21] Following the methods in Rector et al. (2007), color was assigned (B_{435} = blue, V_{606} = yellowish green, I_{814} = red, NUV = purple, and 8 μm = orange) and the images combined using the screen algorithm. Masks were applied to remove the ghost reflection and to reduce the UV emission from the foreground star. Selected regions of the tail were brightened so that they would be visible, because requiring a dark background reduces the contrast of faint astronomical objects.

3. RESULTS AND DISCUSSION

3.1. *SC Candidate Luminosity Functions*

The luminosity function of star clusters can be approximated by a power law, $dN/dL \propto L^{\alpha}$, with $\alpha \approx -2$, in many spirals, starbursts, and merging galaxies (see compilation in Whitmore 2003 and references therein). This strong similarity in the cluster populations across galaxies types and with very different star formation rates led Whitmore (2003) to suggest that the basic properties,

[21] Gnu Image Manipulation Package (GIMP) written by Peter Mattis and Spencer Kimball and released under the GNU General Public License.

such as age, mass, and luminosity, of star cluster systems in nearby, actively star-forming galaxies could be broadly understood from simple statistics. In general, the luminosity of the brightest young cluster (Larsen 2002; Whitmore 2003) in a galaxy scales with the total number of clusters in the system brighter than $M_{\rm V}= -9$, regardless of whether the galaxy is quiescent or starbursting, dwarf or giant, interacting or isolated. Given a universal power-law luminosity function for young star clusters, galaxies with high star formation rates, and therefore larger star cluster populations, are more likely to populate the luminous end of the luminosity function.

In Figure 7, we construct the V_{606} luminosity function for individual galaxies in HCG 31, a dynamical environment with on-going, multiple interactions that is different than those studied previously. The power-law index α is calculated from the best-fit index β in these distributions as: $\alpha = 2.5 \times \beta + 1$, and lies between ≈ -1.8 and -2.3 for each galaxy. To improve statistics, we also summed clusters from all galaxies together to obtain an index $\alpha \approx -2.1$. This is well within the range found for cluster systems in very different galaxies. We show the relationship between the brightest cluster and the total number of clusters with $M_{\rm V_{606}}< -9$ for each galaxy in Figure 8. The line in this figure shows that the best fit relation determined by Whitmore et al. (2007) from 40 galaxies (not including any in compact groups) nicely describes the location of the HCG 31 galaxies in this parameter space. The scatter in HCG 31 is also well within that observed.

The discussion above assumes that dust has not significantly affected the absolute magnitudes of the clusters, and so we consider its potential effects. The brightest clusters in each region are indicated with open stars in the color-color and color-magnitude diagrams for each region (Figs. 9 and 10). Their positions in color space (Fig. 9) are consistent with young ($\tau \lesssim 100$ Myr) or intermediate (τ=100–500 Myr) ages. If we assume that they are actually all very young ($\tau \lesssim 10$ Myr) and are in their current positions as a result of reddening, the inferred extinction would be $A_{606} \lesssim 1$ for all but E, whose colors can accommodate $A_{606} \sim 1.5$). Even in this worst case scenario, the absolute magnitudes of the most luminous clusters would still be consistent with the Whitmore et al. (2007) relation, with the exception of the A+C cluster which would be about a magnitude brighter than the scatter.

In sum, these results suggest that despite the unusual environment of a compact group, there are no obvious differences in the distribution of star cluster luminosities and numbers when compared with more typical environments – which include spirals, starbursts, and mergers – locally.

3.2. *Ages and Spatial Distributions of Star Cluster Candidates*

The age distribution of star clusters provides important information on their formation and disruption, and can be determined by comparing the integrated cluster colors with the predictions of stellar population models. Star cluster candidates have been sorted according to the structures within HCG 31 they are spatially associated with as drawn in Figure 2. From inspection, the majority of the SC candidates are spatially coincident with galaxies and tidal features in HCG 31, with only 4.4% (19 of 424) outside of these boundaries. Furthermore, the SC candidates positions within the color-color plot (Figs. 3 and 9) are generally consistent with instantaneous burst evolutionary tracks. Notably, a large fraction of the brightest clusters in each region are in the lower left section of Figure 3 as expected for the youngest clusters ($\tau \leq 10^7$ yr) and typical of galaxies currently forming stars. The few cluster candidates which fall up and to the left of the region where the nebular emission tracks connect to the rest of the models in the Figure 3 are likely to be $< 10^7$ yr, blue clusters with little nebular emission – clearly a minority of the youngest clusters. Though galaxy A+C is clearly where the largest fraction of young clusters are found, galaxies B and G also have significant populations of young clusters with colors consistent with nebular emission (see Fig. 9).

Many of the cluster candidates in the HCG 31 galaxies fall in a clump in color-color space around V_{606}–$I_{814} \approx 0.4$ and B_{435}–$V_{606} \approx 0.2$, near the region where the tracks which include nebular emission join those which do not. Given the typical photometric errors, the colors of these objects are consistent with ages of 10–500 Myr. In addition, young clusters often have at least modest amounts of extinction associated with them or their parent galaxies, and so younger clusters (without nebular emission) can be pushed into this region. Unfortunately, we are unable to correct for extinction on a cluster by cluster basis because dust reddening is degenerate with age in the filter combination used here. Therefore, we can place only an upper limit on the estimated age of any given cluster that falls along the non-nebular track. Despite this limitation, the color-color diagrams reveal interesting features.

Our cluster sample consists of all objects with $M_{\rm V_{606}} < -9$, where we have only corrected for foreground extinction. Whitmore et al. (1999) have shown that selecting only objects with $M_V \leq -9$ returns a very clean sample of star clusters, because this limit is brighter than all but the most luminous stars. Because clusters fade rapidly with age, a number of them will naturally fade below a given magnitude or luminosity and be lost from the sample. Therefore, this sample is not sensitive to lower mass clusters at older ages (though see §3.4 for a discussion of globular cluster candidates), which can partially explain the lack of many clusters with redder colors.

We can interpret the color (or equivalently, a crude age) distribution of clusters in Figure 3 by considering the results from simple statistical cluster population models (e.g., Whitmore et al. 2007). Specifically, the formation and evolution of star cluster systems can be approximated statistically by following simple formulae, because star cluster systems in galaxies of different types show regularities, such as very similar power-law luminosity functions as discussed above. Chandar, Whitmore, & Fall (in preparation) predict the number of clusters expected for a simple model which assumes that clusters form at a constant rate with an initial power-law mass function, $dN/dM \propto M^{-2}$. Following this simple prescription, *if* no clusters are destroyed and assuming a single V_{606} luminosity limit to mimic our selection procedure, the number of clusters increases each decade in age, by factors of ≈ 2 ($10^7 - 10^8$ yr) and ≈ 4 ($10^8 - 10^9$ yr)

over the number of 10^6-10^7 yr clusters. Even taking into account the dimming of clusters with time, the number of detectable older clusters in bins of 1 dex in $\log(\tau)$ is still expected to grow if no clusters are destroyed. The distribution of cluster colors in HCG 31 galaxies however, shows that the opposite trend is observed, i.e., the number of clusters falls off rapidly with color (age) for HCG 31 galaxies redward of the clump of clusters mentioned above at estimated ages $\approx$few$\times10^7$ yr. Therefore, a scenario with no cluster destruction is not viable unless the star formation rate has increased significantly in the very recent past.

This rapid decline in the number of clusters with redder colors, observed for all of the galaxies, results from a changing history of formation or ongoing disruption of the star clusters, or to some combination of both. A rapid decline in the number of clusters observed with age (or color) has been observed previously in several galaxies, including the Antennae (e.g., Fall et al. 2005; Whitmore et al. 2005), the solar neighborhood (Lada & Lada 2003), and the Small Magellanic Cloud (Chandar et al. 2006). The early, rapid disruption of clusters at ages $\tau \lesssim 10^8$ yr is plausibly dominated by two physical processes internal to the clusters themselves: the disruption of star clusters by the expulsion of interstellar material left over from star formation, and mass-loss from continued stellar evolution (Fall, Chandar, & Whitmore, submitted). Because these internal processes are largely independent of environment, they should disrupt clusters in a similar way in most galaxies. This picture predicts that the number of clusters in a luminosity-limited sample should decline with age (or towards redder colors), very similar to the pattern observed here for several galaxies in HCG 31, even with a constant star formation rate. Therefore, despite the seemingly unusual environment of a compact group, there are no obvious differences in the distribution of star cluster colors, luminosities, and numbers when compared with more typical environments.

An alternative explanation is that all of these galaxies in HCG 31 have experienced a very large, recent, coordinated burst of cluster formation. These galaxies have a range of star formation rates, (see §3.3), that appear to reflect their interaction history. For example, the most actively star-forming galaxies, A and C, are experiencing a direct interaction. Though this interacting/merging galaxy pair is forming stars at a higher rate than galaxy G, and these galaxies do not resemble each other morphologically at all, the general distribution of the clusters colors (ages) is quite similar. In a typical environment, there is no reasonable physical mechanism for coordinating star formation on such large scales given a characteristic speed of bulk motions in the ISM of $\sim 100\,\mathrm{km\,s^{-1}}$. However, in HCG 31, A+C, G, and B as well as the tidal features E, F, and H, are connected by a common H I envelope of tails and bridges, and each region is undergoing a significant rate of star formation given their galaxy types (see §3.3). Therefore, while the SC candidate distributions of colors and luminosities are likely to be significantly shaped by the mechanisms of creation and disruption common to all star-forming galaxies, it is clearly the case that star formation in this group as a whole has been recently elevated as a result of the multiple interactions.

3.3. *Star Formation Rates*

Massive, young stars emit light at UV wavelengths thus offering a direct measure of ongoing star formation. Some fraction of this light is readily absorbed by dust and then re-emitted in the IR. Therefore, UV emission lost to the observer can be recovered using IR data. Following the methodology of Tzanavaris et al. (in preparation), we estimate a total star-formation rate (SFR) as the sum of unobscured (UV-derived) and obscured (IR-derived) components. To the *Spitzer* 24 μm photometry for the HCG 31 galaxies published in Johnson et al. (2007), we applied the calibration of Rieke et al. (2009) to obtain the fraction of star-formation rate (SFR) probed by the IR. Next, we applied the Kennicutt (1998) calibration to the *Swift*/UVOT photometry to obtain the dust-unobscured fraction of the SFR. The sum of these two gives a total SFR effectively corrected for intrinsic dust extinction. Our estimates are listed in Table 3.

The total UV+IR-derived SFR for all galaxies is $\sim$ 10.6 $\mathrm{M_\odot\ yr^{-1}}$, with the largest contribution ($>$ 75%) due to the combined emission from A+C and E (unresolved in the 24 μm *Spitzer* images). This is in reasonable agreement with previous estimates using different SFR indicators, such as Hα, far-IR, 60μm and 1.4 GHz, which give estimates ranging from 2–8 $M_\odot\ \mathrm{yr^{-1}}$ (Dopita et al. 2002; Richer et al. 2003; López-Sánchez et al. 2004; López-Sánchez & Esteban 2007) for the whole group.

As an independent means of constraining the SFR with the new *HST* data, we examined the SC candidates with colors consistent with $\lesssim$ 5 Myr star clusters with nebular emission (see §2.1 and the dashed green line in Fig. 3). Summing the masses of these clusters and dividing by the integrated time on the nebular evolutionary track will give an estimate of the average cluster SFR over this epoch. To convert the colors to an age, the B_{435}–V_{606} vs. V_{606}–I_{814} axes were rotated so that the reddening vector was vertical. For most of the track, the horizontal position in this rotated color space increases monotonically with time. The colors of the SC candidates designated as nebular were then projected onto the nebular evolutionary track, and the distance to the track was recorded as the intrinsic reddening of the cluster. (Negative distances were set to 0.) This gave a mean extinction value for the sample of $A_{606} = 0.74$. The V_{606} magnitude of each SC candidate was then corrected for its intrinsic reddening and converted to a mass using the models (see the dashed curves in Fig. 6). Following this algorithm, we obtained a cluster SFR of $\sim$ 1 $\mathrm{M_\odot\ yr^{-1}}$, approximately an order of magnitude lower than the estimate from the completely independent UV+IR emission. If interpreted literally, this suggests that, given our incompleteness to low mass and highly extincted clusters, at least one-tenth of newly formed stars are still associated with their natal star clusters at these early times. A caveat to this statement is the unknown systematic uncertainty in translating color and magnitude to age and mass.

3.4. *Globular Clusters in HCG 31*

Some of the point sources from Figure 3 are expected to be old ($\tau >$ 10 Gyr) globular clusters (GCs) in the HCG 31 system. Though GCs have been studied in only a few HCGs to date (Barkhouse et al. 2001; Da Rocha

et al. 2002b), they can be used to provide information on the formation and early evolution of such systems (e.g., Brodie & Strader 2006).

Use of color-color diagrams to identify such clusters has proven very effective (e.g., Rhode & Zepf 2001, 2004). The color-color diagram for all point sources with $V_{606} < 26$ (or $M_{V_{606}} < -7.8$ where we expect over 50% completeness for old clusters) in the entire HCG 31 field is plotted in Figure 11. We have relaxed the magnitude limit to $M_{V_{606}} < -7.8$ because for red objects we are not concerned that single stars could be this bright, in contrast to the discussion of the young, blue clusters in §3.1 and §3.2. To define the color range for globular clusters, we have used the reddening corrected $B-V$ and $V-I$ colors for 97 Milky Way globular clusters (those with BVI magnitudes) from the Harris (1996) catalog. The color range $0.55 < (B-V)_0 < 1.05$ and a 0.2 mag wide swath in $(V-I)_0$ centered on the relation $(V-I)_0 = 0.82(B-V)_0 + 0.36$ was found to contain 94% of the clusters. This GC bounding region was then transformed to our ACS filter set (Sirianni et al. 2005) and is shown in Figure 11.

A total of 43 point sources with $V_{606} < 26$. (or $M_{V_{606}} < -7.8$ at the distance of HCG 31) have error ellipses that overlap the bounding region, and are thus considered candidate globular clusters in HCG 31. The vast majority of these objects are centered on the primary galaxies in the group. In A+C, B, and G, they are spread throughout the galaxies, and so the majority of them are not expected to be simply younger, reddened clusters. The latter would be concentrated at the dust emission peaks at the A+C interface and along the western arm of G (see §2.6 and Fig. 1). Although some background elliptical galaxies and foreground Milky Way dwarf stars with similar colors are expected to contaminate our sample, the paucity of such objects over most of the field (coded as 'Other' in Figure 11) shows that the vast majority of objects are likely true GCs in HCG 31. We have used the Besançon Milky Way stellar population model (Robin et al. 2003) to estimate the number of foreground Milky Way stars with magnitudes and colors consistent with our GC selection region; we expect a total of 2 to 3 objects over the entire ACS field for the stellar density of 0.23 objects arcmin^{-2}, consistent with the number of objects (2) that already clearly lie outside the defined HCG 31 regions. Therefore, background contamination is not significant in our candidate GC sample. Inspection of the color-color plot of strictly defined point sources supports our conclusion that the vast majority of objects with nebular colors are marginally resolved; only two point sources with nebular colors (as defined in Figure 3) and $M_{V_{606}} < -9$ satisfy the point source selection criteria.

Studies of GCs in late-type galaxies such as these are made extremely difficult by the rapidly varying background close to the centers of the galaxies, and there is a real possibility that some objects suffer additional internal extinction. As a result, some of our GC candidates may well be younger objects that have been significantly reddened (note the reddening vector in Figure 11). Furthermore, the detection of objects close to the galaxy centers may be adversely affected by photometric incompleteness – the 90% completeness level for point sources within the HCG 31 subsections (see §2.2) are significantly brighter than outside the galaxies.

From inspection of the color-magnitude diagrams for the GC candidates, we find that while many of the candidates are spatially close to their parent galaxies, the large number close to the average 90% completeness limits rather than the brighter galaxy core limits, indicates that the former are more appropriate. As a result, we have adopted a fraction $f = 0.9 \pm 0.1$ for all objects with $V_{606} < 26$. This is certainly not applicable for a small number of objects very close to the galaxy centers, but these will not affect the basic results from our study.

A further test on the effects of incompleteness can be gleaned from the V_{606} luminosity function of the candidates, shown in Figure 12. While the number of GC candidates is small, the luminosity function does show the general property expected for a globular cluster system: a monotonic rise towards the turnover of the GC luminosity function. Also plotted is the expected GC luminosity function assuming a peak at $M_V \sim -7.4$ ($V_{606} = 26.3$ for $DM = 33.83$, $V-I = 1.0 \pm 0.3$), and a dispersion $\sigma = 1.2$ (Harris 2001). That the data continue to rise very sharply to $V_{606} = 26$ again suggests that photometric incompleteness due to varying galactic backgrounds are not strongly affecting our numbers.

From the expected GC luminosity function (as plotted in Figure 12), we estimate that the GCs brighter than $V_{606} = 26$ are 40 ± 7% of the total GC distribution, where the errors reflect added uncertainties of 0.2 mag in the GC luminosity function dispersion, and an uncertainty of 0.2 mag in the location of the peak magnitude. To estimate the total number of GCs in each galaxy in HCG 31, we first correct our observed numbers N_{obs} (and associated Poisson errors) by our bulk completeness fraction $f = 0.9 \pm 0.1$, and then correct for the fraction of the luminosity function we can observe. The final, corrected total number of GC candidates are given in Table 1, where we have also included the single GC candidates superposed on the tidal features E and F. We have made no corrections for the (small) background contamination derived above. Fortunately, both the large distance to HCG 31 and the compactness of the GC systems in these low-mass galaxies mean we are essentially observing the *entire* GC system, and so we make no corrections for any clusters outside the ACS field of view.

Column 6 of Table 1 shows the specific frequency S_N, or the number of GCs normalized to the V-band luminosity $M_V = -15$ (Harris & van den Bergh 1981).[22] The values of S_N for each of the larger galaxies A+C, B and G are all consistent with the lower values expected for late-type galaxies in other environments ($S_N \sim 0.5-0.9$; e.g. Goudfrooij et al. 2003; Chandar et al. 2004; Rhode et al. 2007). From this, there is no evidence that these galaxies have undergone previous mergers that formed a significant population of new massive star cluster populations.

3.5. *Intragroup Stellar Populations?*

[22] While the number of GCs per unit mass (the T parameter from Zepf & Ashman (1993)) is now commonly used to compare numbers of clusters between differing galaxy types, all galaxies in HCG 31 are late-type galaxies and the S_N values can be compared directly.

The lack of a significant number of GC candidates far outside the galaxies may also indicate a dynamically young system, because galaxy interactions are expected to liberate some stars (and star clusters) from the gravitational potentials of their parent galaxies. Indeed, some compact groups do show significant amounts of diffuse light (e.g., Pildis et al. 1995; White et al. 2003; Da Rocha & Mendes de Oliveira 2005; Da Rocha et al. 2008). Does a significant diffuse component (in the form of intergalactic GCs) exist in HCG 31? As there are only two objects that lie significantly outside the small globular cluster systems concentrated in the primary galaxies (broadly consistent with the expected number of foreground Milky Way stars), there is no significant population of intragroup GCs present in our field. However, we can put a meaningful upper limit on the presence of such a population.

To quantify this further, we first assume that both GC candidates outside the galaxies are indeed intragroup systems. We define the fraction of intergalactic cluster light as $f_{IC} = L_{IC}/(L_{gal} + L_{IC})$, where L_{gal} is the combined V-band luminosity of the HCG 31 galaxies and L_{IC} is the total luminosity of the intergalactic GC population. Using the $M_{\rm V}$ value of Conti (1991) converted to our value of the DM, we find a combined $M_{V,group} = -20.7$, or $L_V \sim 15.5 \times 10^9$ $\rm L_{\odot,V}$. Given the two intergalactic GC candidates located far from the HCG galaxies, and subtracting the expected contamination of two stellar objects, we have an observed $N_{IGC,obs}$ consistent with zero, or (correcting for the missing part of the luminosity function) an upper limit of 6 intergalactic GC candidates in the ACS field. Adopting a mean group specific frequency $S_N = 0.6 \pm 0.3$ (appropriate for the late type galaxies in HCG 31), this upper limit corresponds to a V-band luminosity of $\sim 0.9 \times 10^9 L_{\odot,V}$. Thus we place an upper limit of 5% on the intergalactic light in HCG 31. This low value of the intergalactic light fraction, when combined with previous work (where intragroup light fractions in other HCGs can be as high as almost 50%) is suggestive that the range of galactic properties, physical conditions, and dynamical history in the compact group environment may be extremely important in understanding the different processes that shape group evolution.

While our estimate above suggests there is very little (if any) intragroup light in HCG 31, a caveat here is that all galaxies in the group are rather low mass, with compact GC systems concentrated over a small ($r < 10$ kpc) radial extent (Rhode et al. 2007), so while it is possible that the interaction history of HCG 31 is so recent as to not have liberated much of an intergalactic population (consistent with the other observations presented here), it is unclear whether many GCs would be readily removed from such spatially concentrated GC systems in any case.

3.6. *Large-Scale Star Formation*

Star-forming complexes represent the largest units of star formation in a galaxy (see review by Efremov 1995); they are typically kpc-scale regions encompassing several clusters. In local spirals, their masses and sizes approximately follow a power law distribution, and the largest ones scale with the host galaxy's absolute magnitude (Elmegreen et al. 1994, 1996). Complexes form from large-scale gravitational instabilities that depend on the local velocity dispersion, whether the region forms in a disk or a tidal stream. In disk galaxies, the Jeans length is about equal to the disk thickness, and complexes often appear as rather regularly spaced beads of star formation in normal spirals. Because a galaxy's largest complexes can be resolved even in high redshift galaxies, they are useful probes for comparisons of large-scale star formation in a variety of environments. In order to eliminate possible size-of-sample effects (discussed by Selman & Melnick 2000 but disputed by Vicari et al. 2002 and Elmegreen et al. 1994), complexes should be compared among galaxies with comparable absolute magnitudes.

Figure 10 shows a color-magnitude diagram including the HCG 31 complexes, coded according to their regions. Superposed are the evolutionary tracks discussed in Section §2.5. The complexes in region F are too blue in V_{606}–I_{814} for the basic tracks, and require the models that include nebular emission. We have used these tracks for all of the complexes, because a comparison with the Hα image of HCG 31 (Johnson & Conti 2000) shows that all of the complexes are associated with emission. Many of the complexes lie within the Hα knots identified from ground-based images by Iglesias-Paramo & Vilchez (1997). From their positions in the color-magnitude diagram, the inferred complex masses range from $\sim 5 \times 10^5$ to $2 \times 10^7 \rm M_\odot$; overall, the complexes average about $10^6 \rm M_\odot$. The most massive ones are in E and in A+C; two of them in the central regions of A+C probably encompass more than one complex blended along the line-of-sight. The complexes are young, as expected by their Hα emission, with log(ages) ranging from about 6.5 to 7.5 years. The oldest ones are in regions A+C and B, in the central parts of those galaxies, which inference may be due partly to blending with an older background.

The luminosities, L, of individual complexes scale approximately with their diameters, D, as $L \propto D^{1.8}$. This is essentially the same relation as that found for complexes in nearby quiescent spirals (Elmegreen et al. 2006; Elmegreen & Salzer 1999) and also in the gently interacting galaxy pair IC2163/NGC2207 (Elmegreen et al. 2001) at a distance of 35 Mpc. However, the absolute magnitudes of the complexes are ∼2 mag brighter in HCG 31 than in IC 2163/NGC 2207 (even though those galaxies are 1 and 2 magnitudes brighter than HCG 31 A+C, respectively) and in quiescent spirals with comparable or brighter total absolute magnitudes. The masses of the complexes in HCG 31 therefore are also higher, by a factor of ∼5–10. This suggests that the velocity dispersions may be higher in HCG 31 than in IC 2163/NGC 2207. The complex masses in HCG 31 resemble those in blue compact dwarf galaxies, which are also larger than those in normal spiral galaxies with the same absolute magnitudes. This result was inferred to be a consequence of higher disk turbulence in blue compact dwarf galaxies (Elmegreen et al. 1996).

Hα Fabry-Perot observations by Amram et al. (2007) show velocity dispersions of typically 15–20 $\rm km\,s^{-1}$ over most of the regions in HCG 31, with values up to 30 $\rm km\,s^{-1}$ in the vicinity of the complexes. Elevated values in the immediate vicinity of the complexes probably result from extra turbulence generated by associated energetic events such as stellar winds and supernovae. Maps by Richer et al. (2003) with lower spatial and spectral resolution show velocity dispersions of 45 to 95 $\rm km\,s^{-1}$ over the main disk of galaxies A+C, with fairly

constant values of $\sim$50 km s^{-1} in regions B, E, and F, and slightly higher values in region G. Although Hα velocity dispersions do not necessarily reflect the kinematics of the neutral gas out of which the complexes formed, the observed high large-scale Hα velocity dispersions in HCG 31 suggest that the disks and the tidal debris are more turbulent than the 5–10 km s^{-1} typical of quiescent spiral galaxy disks; this is consistent with the presence of more massive complexes.

Star formation is commonly observed in tidal features of interacting galaxies (e.g., Schweizer 1978; Mirabel et al. 1992). Numerical simulations indicate that complexes in such systems can form from interaction-triggered gravitational instabilities in the gaseous component (e.g., Elmegreen et al. 1993; Wetzstein et al. 2007). Complexes observed in tidal tails in the local interacting systems NGC 4485/90 (Elmegreen et al. 1998), the Leo Triplet galaxy NGC 3628 (Chromey et al. 1998), and the Tadpole galaxy UGC10214 (Tran et al. 2003) all have masses of $\sim 10^6$M$_\odot$, similar to those in HCG 31. However, all of these galaxies are 0.6 to 1.3 mag brighter than A+C, the brightest of the HCG 31 galaxies, and so the HCG 31 complexes are more massive relative to their galaxy luminosity.

Another exceptional interacting system is Arp 285, which consists of two galaxies with a tidal tail containing beads of star-forming complexes observed with *Spitzer* (Smith et al. 2008). These galaxies are each $\sim$ 0.8 magnitudes fainter than A+C; their tail clump masses are $< 10^6$ M$_\odot$, but they also contain a bright spot in the disk with 10^8 M$_\odot$.

3.7. *Comparison with Complexes in High Redshift Galaxies*

Complexes have been observed with *HST* in high redshift galaxies in the GEMS and GOODS fields (Elmegreen & Elmegreen 2006; Elmegreen et al. 2007a) and in the Ultra Deep Field (UDF; Elmegreen & Elmegreen 2005; Elmegreen et al. 2005, 2007b, 2009), with sizes in the kpc range. In the standard ΛCDM cosmology (Spergel et al. 2007), 1 kpc corresponds to $\sim 0\farcs13$ at $z = 1$, and has a nearly constant angular size over the redshift range $0.7 < z < 4$. At closer redshifts, the angular size decreases approximately linearly with increasing redshift. With $0\farcs03$ pixels in the ACS images, a kpc-size region corresponds to 3–4 pixels, so complexes much smaller than this could not be measured in the UDF galaxies. On the other hand, if there were complexes significantly larger than this in nearby galaxies, they would be easily discernible. In other words, the largest complexes can be identified and compared in both local and high redshift galaxies. The high z galaxy complexes have masses typically 10^7 to a few $10^8 M_\odot$ from $z = 1 - 4$, decreasing to about 10^6M$_\odot$ at $z = 0.1 - 0.2$, as shown in detail in figures in the previous papers. For the high z cases, masses are estimated by comparing the complex position in color-magnitude space (cf. Fig. 3) and comparing with evolutionary tracks that span a range of reasonable star formation decay rates. In HCG 31, the masses are estimated by comparison with single population, instantaneous burst evolutionary models. Given the colors of the HCG 31 complexes, the inferred masses are not highly sensitive to this assumption which results in a factor of approximately two uncertainty (cf. Fig. 10, Elmegreen et al. 2007a).

Among obviously interacting galaxies, which include M51-type galaxies as well as strongly interacting, gas-rich pairs with long tidal arms (Elmegreen et al. 2007a), the complex masses are 10^5 to $10^{6.5}$ M$_\odot$ at nearby redshifts up to $z = 0.125$, and $10^7 - 10^9$M$_\odot$ at redshifts $1 < z < 1.4$. Faint tidal features are difficult to discern at higher redshifts because of cosmological dimming.

In the GEMS and GOODS samples, galaxies at $z < 0.2$ mostly have rest-frame M_V fainter than –18, because the small volume covered to that depth does not include many intrinsically brighter galaxies; beyond $z = 0.2$, the galaxies measured have rest-frame M_V from –18 to –22. As in local galaxies, the largest complexes are dependent on the absolute (rest-frame) magnitudes of the galaxies, so the main reason the lower redshift GEMS and GOODS complexes are less massive is because their host galaxies are intrinsically fainter. The largest complex masses have a spread of about a factor of 10 for a given absolute rest-frame magnitude, ranging from $\sim 10^{6.5}$M$_\odot$ for rest-frame M_V of –16 to $\sim 10^8$ M$_\odot$ for –20.5 mag (Elmegreen et al., in prep.). These masses are a factor of $\sim$10 larger for a given absolute magnitude than for complexes in local galaxies. In order to compare the complexes in HCG 31 with those in high redshift galaxies, a Gaussian blur of 30 pixels was applied to the HCG 31 images, corresponding to pixels covering about 250 pc. This scale simulates its appearance if at $1 < z < 4$.

The HCG 31 complexes were re-measured based on their boundaries in the blurred images. Some complexes were not recognizable in the blurred images because they were too faint or too small; a few were blended with other complexes that were too close. Most of the lowest mass complexes disappear, although the remaining complexes still range from $\sim 10^5$ to $10^{7.3}$ M$_\odot$. A comparison of the full resolution and blurred complexes shows that the blurred ones typically are only $\sim$20% more massive, even when they contain blended complexes; the colors differ by at most $\sim$ 0.2 mag, so the inferred ages are about the same. The diameters range from about 300 to 650 pc (in one case, the diameter measured was smaller than in the unblurred image, due to uncertainty in placing the boundary.) These complexes are similar in mass and size to those in the interacting GEMS and GOODS galaxies of comparable rest-frame magnitudes.

The larger masses in the high redshift galaxies are presumed to be the result of high turbulence in the disks; for example, kinematics inferred from spectroscopic observations of a $z = 1.6$ galaxy, UDF6462, indicates velocity dispersions of 40 km s^{-1} (Bournaud et al. 2008), while numerical simulations reproducing the large-scale star formation (Bournaud et al. 2007) also require values several times higher than in local quiescent galaxies.

Thus, the complexes in HCG 31 can be understood in terms of large-scale star formation from gravitational instabilities in the gas driven by turbulence. Their sizes are comparable to what is expected based on complexes in nearby spirals. Their masses are similar to those in $z \sim 1$ galaxies of comparable magnitude, and are intermediate between the smaller ones found in gently interacting nearby systems and the larger ones found in presumably more turbulent high redshift counterparts.

3.8. *Underlying Stellar Populations*

An outstanding issue from previous *HST* studies is whether F contains an older stellar population in addition to the current generation of young stars. From an examination of the region-specific color-color plot (Fig. 9), none of the star cluster candidates or complexes in F have colors consistent with > 1 Gyr populations, and there is only one globular cluster candidate within the larger F boundary. In general, it is hard to see individual, old stars directly (with the exception of GCs), due to their faintness. The diffuse light within galaxies offers an opportunity to study fainter stellar populations than those described in the previous sections and can give us a handle on the population of older stars.

To search for a distributed, underlying, older stellar population, we examined a processed B_{435}–I_{814} image of the entire ACS field of view. The image, presented in Figure 13, was created from the point-source subtracted images generated by the SC candidate PSF-fitting photometry. It has been Vega-magnitude calibrated and boxcar-smoothed (with a 13 pix [180 pc] window) and corrected for Galactic extinction. We use B_{435}–I_{814} to remove the confusion of nebular emission prominent in V_{606}, and also because B_{435}–$I_{814} \gtrsim 1.0$ is a good indicator of stellar populations with ages > 500 Myr, barring intrinsic reddening (see Figure 13).

In actively star forming galaxies, the diffuse light will be a mix of different stellar populations. We might expect the light to be dominated by the youngest (and also brightest) stars that are present. Therefore, we will typically be able to put a lower limit on the age of stars contributing to the diffuse light in the galaxies.

From inspection, diffuse tidal debris with B_{435}–$I_{814}\sim$0.4–0.8 apparently pulled out from A+C is evident to the north, as is some debris stretching to the south and overlapping with E and H. These colors are consistent with stellar ages > 100 Myr in this debris. The overall colors of A+C and B are in the range B_{435}–I_{814}=0.4–1.0, with bluer (B_{435}–I_{814}=–0.1 to 0.4) regions coincident with the locations of the youngest SC candidates. While the inner disk of G is blue (B_{435}–$I_{814}\sim$ 0.4), the location of the complexes to the west stand out with B_{435}–$I_{814}\sim$–0.1 to 0.4. The outer disk of G is significantly redder than the other structures in the group, with B_{435}–I_{814}=0.7–1.2. From the B_{435}–I_{814} color-magnitude diagram (Fig. 14) this indicates that the intermediate age range in A+C, B, and G is at least several 100 Myr, up to ∼ 1 Gyr. The presence of GC candidates (§3.4) also supports the presence of ancient stars in these galaxies.

Notably, F shows no evident diffuse emission consistent with an older stellar population; the reddest regions have B_{435}–$I_{814}\sim$ 0.2–0.3, consistent with stars < 10 Myr. Given the low surface brightness of this material, it cannot be hiding a substantial population of old stars. While we cannot rule out that there is some low level stellar population with ages of 100 Myr and older, these observations show no evidence for such a population, and probably give the best evidence to date that F started forming stars only recently. This implies that the material comprising F is almost entirely 'fresh', and F is overall a very young structure.

4. SUMMARY AND CONCLUSIONS

4.1. *Modes of Star Formation*

An in-depth examination of the colors of structures at all scales of star formation, from compact star cluster candidates, to large star-forming clusters, to the diffuse underlying emission, indicates that the entire HCG 31 system is suffused with recent and ongoing star formation. Star cluster candidates with nebular colors are present throughout HCG 31, specifically concentrated in the inner disk and western ring of G, through the midplane of B, in the interaction region of A+C, and across E, H, and F. While the prominence of SC candidates with nebular colors is not sufficient evidence of a recent enhancement of star formation activity, other available information points in that direction. In particular, while the SFR is enhanced relative to galaxies with similar masses, the sum total of H I in the system is not noticeably depleted. Crudely, this sets an upper limit to the timescale of enhanced star formation of ∼ 300 Myr, as in this amount of time a significant fraction (∼ 20%) of the H I would have been converted to stars. Furthermore, the tight constraints on intragroup GC candidates and diffuse light, and the consistency of the GC luminosity distribution with the *low end* of that expected for similar galaxies argue against previous epochs of interaction-triggered star formation. In simulations of mergers of pairs of bulgeless disk galaxies, the typical timescale for the SFR to be elevated by an order of magnitude or so is ∼ 150 Myr, and the most intense burst is triggered shortly after the first encounter (Mihos & Hernquist 1996). If these results are applicable to the more complicated dynamics of the compact group environment, then the ongoing burst may be of quite recent vintage. The current high rate of star formation is not sustainable long term (at most a Gyr or so) given the finite reservoir of cold gas of 1.6×10^{10} $M_\odot$ (Verdes-Montenegro et al. 2005).

On the scales of star clusters, both young and globular, the HCG 31 system is consistent with local galaxies of similar star formation rates and masses, as shown by the luminosity functions (Figs. 7 and 12). Furthermore, the values of brightest cluster $M_{V_{606}}$ as a function of number for distinct regions in HCG 31 match those of galaxies in the local Universe with a range of properties (Fig. 8). This supports the claim that star cluster formation (and destruction) follow universal patterns that scale with star formation rate, but are otherwise insensitive to their large-scale environment.

However, the SC candidate populations of all compact groups studied to date are not the same. Stephan's Quintet (HCG 92) is another Hickson Compact Group with active star formation as a result of strong gravitational interactions (e.g., Xu et al. 1999; Sulentic et al. 2001). Specifically, the galaxy NGC 7318b is blueshifted by 900 $\mathrm{km\,s^{-1}}$ with respect to the rest of the group galaxies, and is currently ploughing through the neutral intragroup medium (Shostak et al. 1984). This has triggered a large-scale (∼ 40 kpc) ridge of star formation coincident with a radio and X-ray bright shock (e.g., van der Hulst & Rots 1981; Pietsch et al. 1997; Trinchieri et al. 2003). With *HST* WFPC2 three-color imaging, Gallagher et al. (2001) identified a population of young, luminous SC candidates that traces the large-scale shock. In contrast to HCG 31, however, none of these SC candidates has colors consistent with strong nebular emission, though clusters apparently as young as ∼ 2–3 Myr are seen. Af-

ter accounting for the brighter absolute magnitude limit and different filters of the WFPC2 observations, SC candidates in Stephan's Quintet with comparable colors and absolute magnitudes (of $M_V < -10$) to those in HCG 31 would have been detected if present. There are in total ~ 30 star cluster candidates in Stephan's Quintet with comparably young ages ($\tau \lesssim 10$ Myr), the vast majority of which lie along the large-scale shock. From *Spitzer* spectroscopy of the shock ridge, strong, broad H_2 emission lines, weak polycyclic aromatic hydrocarbon emission, and very low excitation ionized gas tracers speak to the unusual environment of the region (Appleton et al. 2006). This setting may be one in which the interstellar medium of young clusters is rapidly stripped, and thus young clusters do not have cocoons of gas to photoionize. However, though the young, compact star clusters are apparently not strong Hα emitters, optical spectra of bright H II regions do show prominent emission lines (e.g., Mendes de Oliveira et al. 2004).

On the kiloparsec scales of complexes, HCG 31 hosts a population with masses that more closely resemble those found at higher redshifts. This suggests that, similar to galaxies at $z = 1$–2 with similar absolute magnitudes, the disks of galaxies in HCG 31 have higher turbulent velocities than typically found in the local universe. This most plausibly arises because of the ongoing multigalaxy interactions in the system. In this sense therefore, the larger-scale star formation structures are reminiscent of those seen during the epoch of morphological galaxy transformations in dense environments.

4.2. *Dwarf Galaxy Candidates*

Previous optical photometry suggested that galaxy F, composed of two separate H I peaks within the same cloud, is comprised of only a young population and that given its location in the tidal tail of the A+C complex it is likely a recently formed structure undergoing its first burst of star formation (Johnson & Conti 2000). Richer et al. (2003) find that galaxies E and F have similar oxygen abundances to A+C, verifying that they have been tidally removed from the A+C complex. The stellar populations are younger than the travel time from the A+C complex, and clearly are forming *in situ* (Mendes de Oliveira et al. 2006).

Amram et al. (2004, 2007) found a flat / shallow rotation velocity in E and F using optical Fabry-Perot data, and thus classify them as tidal debris though dwarf galaxies are expected to be slow rotators (Mendes de Oliveira et al. 2006). While E and H are merely fragments which are likely to fall back into A+C, F and R have H I column densities and Hα luminosities consistent with being true dwarf galaxies, and given their positions are less likely to fall back into the A+C complex.

From the colors and luminosities of the SC candidates and complexes, the total stellar mass in F is $\gtrsim 10^6 M_\odot$. While this is within the range found for dwarf galaxies, it is unclear whether it is sufficient to establish F as an independent entity within this compact group. From our analysis of the faint, diffuse emission in F, we find no evidence for an older stellar population, consistent with the Johnson & Conti (2000) analysis.

4.3. *Future Evolution*

The multiple interactions of low mass galaxies that characterize the HCG 31 system are evocative of hierarchical structure formation in process, and so we consider the likely end result, and compare it to early type systems in the local Universe that presumably underwent this type of dynamical processing at earlier times ($z \gtrsim 1$). We thus examine if HCG 31 can be cast accurately as a local analogue of high-redshift hierarchical structure formation.

At present, the sum of H I in HCG 31 as a whole is consistent with that expected from its member galaxies based on their magnitudes and morphologies (Williams et al. 1991; Verdes-Montenegro et al. 2001), though a large fraction of that gas has been pulled out from the individual galaxies into tidal structures. This suggests that HCG 31 has recently contracted as the gas has not yet been significantly reduced by a long period of star formation. The low radial velocity dispersions of the five primary galaxies (A, B, C, G, and Q) and the projected lengths of the H I tails are generally consistent with a bound system (Mendes de Oliveira et al. 2006). It seems quite likely that the individual galaxies in this group will ultimately merge into a single elliptical, as predicted by Rubin et al. (1990), in a wet merger process. Subsequently, it is not likely to move along the red sequence to higher luminosities as there are no candidates for future dry mergers in the neighborhood. We then consider whether this system will become a so-called 'fossil group': the putative remnant of a coalesced compact group.

A key component of the fossil group definition is a hot, extended X-ray medium with $L_X \geq 0.5 \times 10^{42} h_{70}^{-2}$ erg s^{-1} (Jones et al. 2003). At present, HCG 31 has little extended X-ray emission. Unlike in galaxy clusters and massive groups, the gravitational potential of HCG 31 given its velocity dispersion is not sufficient to virialize gas to X-ray emitting temperatures. Therefore, the only possible source of heating is star formation whereby the mechanical energy from supernovae and stellar winds is thermalized into $\sim 10^6$ K gas. We can make a crude estimate of the potential X-ray luminosity (excluding compact sources) generated by conversion of the available reservoir of neutral gas into stars. In the following argument, we use the numbers from Mihos & Hernquist (1996) for the efficiencies of gas-to-star and supernova-to-kinetic energy conversions. If 75% of the $1.6 \times 10^{10} M_\odot$ of H I is converted to stars, then $\sim 9 \times 10^7$ supernovae are expected assuming the initial mass function of §2.5. If 10^{-4} is the fraction of supernova energy converted to kinetic energy, and all of that energy is ultimately radiated as X-rays, the integrated X-ray energy of all supernova (assuming $E_{SN} = 10^{51}$ ergs) is 9×10^{54} ergs. Over the course of a 150 Myr star formation episode, the power would thus be 2×10^{39} erg s^{-1}, or approximately 0.4% of the minimum for a fossil group. Empirically, the diffuse emission from star formation observed locally is 1–5×10^{39} erg s^{-1}/($M_\odot$ yr^{-1}) (Owen & Warwick 2009), and so this estimate is not unreasonable. The total dynamical (including dark matter) mass of HCG 31 from H I velocities (assuming spherical symmetry and dynamical relaxation; Verdes-Montenegro et al. 2005) is 2×10^{11} $M_\odot$, approximately two orders of magnitude smaller than the dark matter halo mass of the lower mass (and lower X-ray luminosity) fossil groups (e.g., Díaz-Giménez et al. 2008). Therefore, HCG 31 is a plausible candidate for a

low mass fossil group, where fossil group here applies to the dynamical history of a system rather than the specific X-ray luminosity criteria as defined by Jones et al. (2003).

We can also consider the current population of globular clusters, and investigate how that compares to those of low mass ellipitical galaxies in the local universe. While our value of $S_{\rm N} = 0.6$ for a galaxy with $M_{\rm V} = -20.7$ ($L_{\rm V} = 1.6 \times 10^{10} {\rm L}_{\odot}$) would be low for an elliptical of this absolute magnitude, late type galaxies have lower mass-to-light ratios, and therefore lower values of $S_{\rm N}$ even with the same number of clusters per unit stellar mass. A globular cluster system studied previously in NGC 6868, an E2 galaxy in the Telescopium group ($\sigma \sim 250$ km s^{-1}) with evidence of somewhat recent merger activity, has $S_{\rm N} = 1.1$, a value on the low end for ellipticals (Da Rocha et al. 2002a). Could such a galaxy be the result of a coalesced HCG 31?

To compare globular cluster systems in galaxies of different type, it is more convenient to use the T parameter, defined as the number of old globular clusters per unit stellar mass (Zepf & Ashman 1993). Assuming values of $M/L_{\rm V}$=10 and 3 for ellipticals and late-type spirals, respectively, we obtain $T = 1.7 \pm 0.8$ for HCG 31 assuming a total globular cluster population of 111 ± 51 for the entire system and a mass of 6×10^{10} M$_{\odot}$. The corresponding T value for NGC 6868 ($M_{\rm V} = -21.9$; $L_{\rm V} = 5 \times 10^{10}$ L$_{\odot}$; $M = 49 \times 10^{10}$ M$_{\odot}$) using the globular cluster numbers from Da Rocha et al. (2002a) is 2.2 ± 1.1. Using $M_{\rm V} = -22.17$ (Forbes et al. 2007) for NGC 6868 gives $T = 1.7 \pm 0.9$. Therefore, correcting for the differing mass-to-light ratios of the two systems makes them fully consistent within the uncertainties. Note that the T value for HCG 31 would likely be a lower limit, given that it is currently forming new star clusters, some with masses $\gtrsim 10^5$M$_{\odot}$(see Fig. 10); these massive clusters would only increase the T value if they survive the next few Gyrs intact.

In sum, the likely outcome is that HCG 31 will have too low a mass and insufficient X-ray luminosity to meet the Jones et al. (2003) criteria for classification as a fossil group at $z = 0$. However, in terms of dynamical evolution and $L_{\rm X}$ vs. halo mass, it could plausibly extend the relation seen in fossil groups to lower masses. The globular cluster populations of local ellipticals of similar mass to HCG 31, however, are consistent with the current population of globular clusters in HCG 31 even if the ongoing star formation does not boost their numbers. HCG 31 therefore does enable us to investigate hierarchical structure formation – the formation of a single elliptical from several smaller and gas-rich galaxies – in a local setting, though the likely result will be a smaller version of the end products of putative group coalescence that currently exist in the local Universe.

Support for this work was provided by NASA through grant number HST-GO-10787.15-A from the Space Telescope Science Institute which is operated by AURA, Inc., under NASA contract NAS 5-26555, and the National Science and Engineering Research Council of Canada (SCG). We thank Konstantin Fedotov for a careful reading of the paper, and the anonymous referee for constructive comments that improved this paper.

REFERENCES

Amram, P., Mendes de Oliveira, C., Plana, H., Balkowski, C., & Hernandez, O. 2007, A&A, 471, 753
Amram, P., et al. 2004, ApJ, 612, L5
Appleton, P. N., et al. 2006, ApJ, 639, L51, arXiv:astro-ph/0602554
Balogh, M. L., Baldry, I. K., Nichol, R., Miller, C., Bower, R., & Glazebrook, K. 2004, ApJ, 615, L101, arXiv:astro-ph/0406266
Barkhouse, W. A., West, M. J., & Bothun, G. D. 2001, ApJ, 562, 679, arXiv:astro-ph/0107491
Bertin, E. & Arnouts, S. 1996, A&AS, 117, 393
Bournaud, F., Elmegreen, B. G., & Elmegreen, D. M. 2007, ApJ, 670, 237, arXiv:0708.0306
Bournaud, F., et al. 2008, A&A, 486, 741, arXiv:0803.3831
Brodie, J. P. & Strader, J. 2006, ARA&A, 44, 193, arXiv:astro-ph/0602601
Bruzual, G. & Charlot, S. 2003, MNRAS, 344, 1000
Calzetti, D., et al. 2007, ApJ, 666, 870, 0705.3377
Cardelli, J. A., Clayton, G. C., & Mathis, J. S. 1989, ApJ, 345, 245
Chandar, R., Fall, S. M., & Whitmore, B. C. 2006, ApJ, 650, L111, arXiv:astro-ph/0609360
Chandar, R., Whitmore, B., & Lee, M. G. 2004, ApJ, 611, 220, arXiv:astro-ph/0407460
Chromey, F. R., Elmegreen, D. M., Mandell, A., & McDermott, J. 1998, AJ, 115, 2331
Conti, P. S. 1991, ApJ, 377, 115
Conti, P. S., Leitherer, C., & Vacca, W. D. 1996, ApJ, 461, L87+, arXiv:astro-ph/9602084
Cooper, M. C., et al. 2007, MNRAS, 376, 1445, arXiv:astro-ph/0607512
Cucciati, O., et al. 2006, A&A, 458, 39
Da Rocha, C., de Oliveira, C. M., Bolte, M., Ziegler, B. L., & Puzia, T. H. 2002a, AJ, 123, 690
Da Rocha, C. & Mendes de Oliveira, C. 2005, MNRAS, 364, 1069, arXiv:astro-ph/0509908
Da Rocha, C., Mendes de Oliveira, C., Bolte, M., Ziegler, B. L., & Puzia, T. H. 2002b, AJ, 123, 690
Da Rocha, C., Ziegler, B. L., & Mendes de Oliveira, C. 2008, MNRAS, 388, 1433, 0805.4015
Díaz-Giménez, E., Muriel, H., & Mendes de Oliveira, C. 2008, A&A, 490, 965, 0809.2290
Dopita, M. A., Pereira, M., Kewley, L. J., & Capaccioli, M. 2002, ApJS, 143, 47
Dressler, A. 1980, ApJ, 236, 351
Dressler, A., et al. 1997, ApJ, 490, 577
Efremov, Y. N. 1995, AJ, 110, 2757
Elmegreen, B. G. & Elmegreen, D. M. 2005, ApJ, 627, 632, arXiv:astro-ph/0504032
Elmegreen, B. G., Elmegreen, D. M., Fernandez, M. X., & Lemonias, J. J. 2009, ApJ, 692, 12, 0810.5404
Elmegreen, B. G., Elmegreen, D. M., Salzer, J. J., & Mann, H. 1996, ApJ, 467, 579
Elmegreen, B. G., Kaufman, M., & Thomasson, M. 1993, ApJ, 412, 90
Elmegreen, D. M., Chromey, F. R., Knowles, B. D., & Wittenmyer, R. A. 1998, AJ, 115, 1433
Elmegreen, D. M. & Elmegreen, B. G. 2006, ApJ, 651, 676, arXiv:astro-ph/0607579
Elmegreen, D. M., Elmegreen, B. G., Ferguson, T., & Mullan, B. 2007a, ApJ, 663, 734, arXiv:0704.0911
Elmegreen, D. M., Elmegreen, B. G., Kaufman, M., Sheth, K., Struck, C., Thomasson, M., & Brinks, E. 2006, ApJ, 642, 158, arXiv:astro-ph/0605524
Elmegreen, D. M., Elmegreen, B. G., Lang, C., & Stephens, C. 1994, ApJ, 425, 57
Elmegreen, D. M., Elmegreen, B. G., Ravindranath, S., & Coe, D. A. 2007b, ApJ, 658, 763
Elmegreen, D. M., Elmegreen, B. G., Rubin, D. S., & Schaffer, M. A. 2005, ApJ, 631, 85, arXiv:astro-ph/0508216
Elmegreen, D. M., Kaufman, M., Elmegreen, B. G., Brinks, E., Struck, C., Klarić, M., & Thomasson, M. 2001, AJ, 121, 182
Elmegreen, D. M. & Salzer, J. J. 1999, AJ, 117, 764

Fall, S. M., Chandar, R., & Whitmore, B. C. 2005, ApJ, 631, L133, arXiv:astro-ph/0509293
Forbes, D. A., Proctor, R., Strader, J., & Brodie, J. P. 2007, ApJ, 659, 188, arXiv:astro-ph/0612415
Franzetti, P., et al. 2007, A&A, 465, 711, arXiv:astro-ph/0607075
Gallagher, S. C., Charlton, J. C., Hunsberger, S. D., Zaritsky, D., & Whitmore, B. C. 2001, AJ, 122, 163
Gallagher, S. C., Johnson, K. E., Hornschemeier, A. E., Charlton, J. C., & Hibbard, J. E. 2008, ApJ, 673, 730
Gooch, R. 1996, in Astronomical Data Analysis Software and Systems V, eds. G. H. Jacoby & J. Barnes, vol. 101 of *Astronomical Society of the Pacific Conference Series*, 80–+
Goudfrooij, P., Strader, J., Brenneman, L., Kissler-Patig, M., Minniti, D., & Edwin Huizinga, J. 2003, MNRAS, 343, 665, arXiv:astro-ph/0304195
Harris, W. E. 1996, AJ, 112, 1487
— 2001, in Saas-Fee Advanced Course 28: Star Clusters, eds. L. Labhardt & B. Binggeli, 223–+
Harris, W. E. & van den Bergh, S. 1981, AJ, 86, 1627
Hickson, P. 1993, Astrophysical Letters Communications, 29, 1
Hickson, P., Mendes de Oliveira, C., Huchra, J. P., & Palumbo, G. G. 1992, ApJ, 399, 353
Hogg, D. W., et al. 2004, ApJ, 601, L29, arXiv:astro-ph/0307336
Iglesias-Paramo, J. & Vilchez, J. M. 1997, ApJ, 479, 190
Johnson, K. E. & Conti, P. S. 2000, AJ, 119, 2146
Johnson, K. E., Hibbard, J. E., Gallagher, S. C., Charlton, J. C., Hornschemeier, A. E., Jarrett, T. H., & Reines, A. E. 2007, AJ, 134, 1522
Johnson, K. E., Vacca, W. D., Leitherer, C., Conti, P. S., & Lipscy, S. J. 1999, AJ, 117, 1708
Jones, L. R., Ponman, T. J., Horton, A., Babul, A., Ebeling, H., & Burke, D. J. 2003, MNRAS, 343, 627, arXiv:astro-ph/0304257
Kennicutt, R. C., Jr. 1998, ARA&A, 36, 189
Kennicutt, R. C., Jr., et al. 2003, PASP, 115, 928
Kunth, D. & Schild, H. 1986, A&A, 169, 71
Lada, C. J. & Lada, E. A. 2003, ARA&A, 41, 57, arXiv:astro-ph/0301540
Larsen, S. S. 2002, AJ, 124, 1393, arXiv:astro-ph/0206295
Leitherer, C., et al. 1999, ApJS, 123, 3
López-Sánchez, Á. R. & Esteban, C. 2007, ArXiv e-prints, 0704.2846
López-Sánchez, Á. R., Esteban, C., & Rodríguez, M. 2004, ApJS, 153, 243
Maraston, C. 2005, MNRAS, 362, 799, arXiv:astro-ph/0410207
Mendes de Oliveira, C., Cypriano, E. S., Sodré, L., Jr., & Balkowski, C. 2004, ApJ, 605, L17
Mendes de Oliveira, C. L., Temporin, S., Cypriano, E. S., Plana, H., Amram, P., Sodré, L. J., & Balkowski, C. 2006, AJ, 132, 570
Meyer, M. J., et al. 2004, MNRAS, 350, 1195
Mihos, J. C. & Hernquist, L. 1996, ApJ, 464, 641, arXiv:astro-ph/9512099
Mirabel, I. F., Dottori, H., & Lutz, D. 1992, A&A, 256, L19
Owen, R. A. & Warwick, R. S. 2009, MNRAS, 275
Pietsch, W., Trinchieri, G., Arp, H., & Sulentic, J. W. 1997, A&A, 322, 89
Pildis, R. A., Bregman, J. N., & Schombert, J. M. 1995, AJ, 110, 1498, arXiv:astro-ph/9507039
Rector, T. A., Levay, Z. G., Frattare, L. M., English, J., & Pu'uohau-Pummill, K. 2007, AJ, 133, 598, arXiv:astro-ph/0412138
Rejkuba, M., Greggio, L., Harris, W. E., Harris, G. L. H., & Peng, E. W. 2005, ApJ, 631, 262
Rhode, K. L. & Zepf, S. E. 2001, AJ, 121, 210
— 2004, AJ, 127, 302
Rhode, K. L., Zepf, S. E., Kundu, A., & Larner, A. N. 2007, AJ, 134, 1403
Richer, M. G., Georgiev, L., Rosado, M., Bullejos, A., Valdez-Gutiérrez, M., & Dultzin-Hacyan, D. 2003, A&A, 397, 99, arXiv:astro-ph/0211033
Rieke, G. H., Alonso-Herrero, A., Weiner, B. J., Pérez-González, P. G., Blaylock, M., Donley, J. L., & Marcillac, D. 2009, ApJ, 692, 556
Robin, A. C., Reylé, C., Derrière, S., & Picaud, S. 2003, A&A, 409, 523, arXiv:astro-ph/0401052
Rubin, V. C., Hunter, D. A., & Ford, W. K. J. 1990, ApJ, 365, 86
Salzer, J. J., Jangren, A., Gronwall, C., Werk, J. K., Chomiuk, L. B., Caperton, K. A., Melbourne, J., & McKinstry, K. 2005, AJ, 130, 2584
Schlegel, D. J., Finkbeiner, D. P., & Davis, M. 1998, ApJ, 500, 525, arXiv:astro-ph/9710327
Schweizer, F. 1978, in Structure and Properties of Nearby Galaxies, eds. E. M. Berkhuijsen & R. Wielebinski, vol. 77 of *IAU Symposium*, 279–284
Selman, F. J. & Melnick, J. 2000, ApJ, 534, 703
Shostak, G. S., Allen, R. J., & Sullivan, W. T., III 1984, A&A, 139, 15
Sirianni, M., et al. 2005, PASP, 117, 1049
Smith, B. J., et al. 2008, AJ, 135, 2406, 0803.4218
Spergel, D. N., et al. 2007, ApJS, 170, 377
Stetson, P. B. 1987, PASP, 99, 191
Sulentic, J. W., Rosado, M., Dultzin-Hacyan, D., Verdes-Montenegro, L., Trinchieri, G., Xu, C., & Pietsch, W. 2001, AJ, 122, 2993
Tran, H. D., et al. 2003, ApJ, 585, 750, arXiv:astro-ph/0211371
Trinchieri, G., Sulentic, J., Breitschwerdt, D., & Pietsch, W. 2003, A&A, 401, 173
Vacca, W. D. & Conti, P. S. 1992, ApJ, 401, 543
van der Hulst, J. M. & Rots, A. H. 1981, AJ, 86, 1775
Verdes-Montenegro, L., Del Olmo, A., Yun, M. S., & Perea, J. 2005, A&A, 430, 443
Verdes-Montenegro, L., Yun, M. S., Williams, B. A., Huchtmeier, W. K., Del Olmo, A., & Perea, J. 2001, A&A, 377, 812
Vicari, A., Battinelli, P., Capuzzo-Dolcetta, R., Wyder, T. K., & Arrabito, G. 2002, A&A, 384, 24
Walker, L. M., Johnson, K. E., Gallagher, S. C., Hibbard, J. E., Hornschemeier, A. E., Charlton, J. C., Young, J., Gronwall, C., & Jarrett, T. H., 2009, AJ, submitted
Wetzstein, M., Naab, T., & Burkert, A. 2007, MNRAS, 375, 805, arXiv:astro-ph/0510821
White, P. M., Bothun, G., Guerrero, M. A., West, M. J., & Barkhouse, W. A. 2003, ApJ, 585, 739
Whitmore, B. C. 2003, in A Decade of Hubble Space Telescope Science, eds. M. Livio, K. Noll, & M. Stiavelli, 153–178
Whitmore, B. C., Chandar, R., & Fall, S. M. 2007, AJ, 133, 1067, arXiv:astro-ph/0611055
Whitmore, B. C., Zhang, Q., Leitherer, C., Fall, S. M., Schweizer, F., & Miller, B. W. 1999, AJ, 118, 1551
Whitmore, B. C., et al. 2005, AJ, 130, 2104
Williams, B. A., McMahon, P. M., & van Gorkom, J. H. 1991, AJ, 101, 1957
Williams, B. A. & Rood, H. J. 1987, ApJS, 63, 265
Willmer, C. N. A., et al. 2006, ApJ, 647, 853, arXiv:astro-ph/0506041
Xu, C., Sulentic, J. W., & Tuffs, R. 1999, ApJ, 512, 178
Zabludoff, A. I., & Mulchaey, J. S. 2000, ApJ, 539, 136
Zabludoff, A. I., & Mulchaey, J. S. 1998, ApJ, 496, 39
Zabludoff, A. I., Zaritsky, D., Lin, H., Tucker, D., Hashimoto, Y., Shectman, S. A., Oemler, A., & Kirshner, R. P. 1996, ApJ, 466, 104
Zepf, S. E. & Ashman, K. M. 1993, MNRAS, 264, 611

TABLE 1
Star Cluster and Globular Cluster Candidate Data[a]

Region	$M_{B_{435}}$[b]	$B-V$[c]	N_{comp}[d]	N_{SCCs}[e]	f_{neb}[f]	$M_{V_{606}}$(brightest)[g]	N_{GCCs}[h]	S_N[i]
A+C	–20.0	0.03	11	178	0.29	–15.5	50 ± 26	0.5 ± 0.3
B	–18.5	0.17	11	105	0.23	–13.4	39 ± 22	1.3 ± 0.7
E	–16.5	–0.03	3	17	0.35	–11.6	(3)	(0.3)
F	–15.8	–0.08	4	16	0.75	–11.4	(3)	(0.5)
G	–18.9	–0.01	11	86	0.33	–13.4	20 ± 13	0.6 ± 0.4
H	···	···	0	3	0.67	–11.2	0	0

[a]The magnitudes in this table have been corrected for Galactic extinction only.
[b]Absolute magnitude for the entire region.
[c]The $B-V$ color for each region is reproduced from Table 2 of López-Sánchez et al. (2004).
[d]The number of complexes in each region (see §2.3).
[e]The number of star cluster candidates in each region (see §2.1).
[f]The fraction of star cluster candidates in each region with colors consistent with nebular emission (see §2.1 and the lefthand panel of Fig. 3).
[g]The absolute magnitude, $M_{V_{606}}$, of the brightest SC candidate in each region. The magnitude has not been corrected for intrinsic extinction.
[h]The total calculated number of globular cluster candidates after correction for incompleteness (see §3.4). The numbers in parentheses were estimated from only one object.
[i]The specific frequency of globular cluster candidates (see §3.4). The numbers in parentheses were calculated from only one object.

TABLE 2
Star-forming Complexes

Region	Complex	RA	Dec	$M_{V_{606}}$	B_{435}–V_{606}	V_{606}–I_{814}	Diameter (pc)
A+C	1	5:01:39.7676	-4:15:11.865	−14.09	0.31	0.23	539
A+C	2	5:01:38.6204	-4:15:14.205	−13.25	0.25	0.47	331
A+C	3	5:01:38.4399	-4:15:13.545	−13.88	0.26	0.16	452
A+C	4	5:01:38.0909	-4:15:24.225	−14.75	0.20	0.26	414
A+C	5	5:01:38.7127	-4:15:32.985	−15.37	0.47	0.64	306
A+C	6	5:01:38.2434	-4:15:33.285	−15.20	0.41	0.38	271
A+C	7	5:01:37.7319	-4:15:32.715	−15.81	0.85	−0.38	198
A+C	8	5:01:37.6858	-4:15:32.745	−14.71	0.60	−0.09	191
A+C	9	5:01:37.8062	-4:15:27.945	−17.73	0.51	−0.21	489
A+C	10	5:01:37.7500	-4:15:28.965	−15.77	0.36	−0.00	265
A+C	11	5:01:37.7019	-4:15:31.305	−17.01	0.27	−0.04	418
B	1	5:01:34.7918	-4:16:00.254	−14.34	0.38	−0.12	288
B	2	5:01:35.3112	-4:15:47.414	−13.71	0.32	0.39	274
B	3	5:01:35.2350	-4:15:50.534	−13.06	0.47	0.20	166
B	4	5:01:35.5840	-4:15:41.834	−13.52	0.51	0.18	265
B	5	5:01:35.8327	-4:15:40.334	−13.84	0.62	−0.21	265
B	6	5:01:35.7685	-4:15:40.154	−13.00	0.43	0.10	207
B	7	5:01:35.8327	-4:15:42.614	−12.54	0.77	−0.31	133
B	8	5:01:35.9169	-4:15:42.314	−13.34	0.31	0.18	257
B	9	5:01:35.7966	-4:15:44.114	−12.50	0.27	0.42	166
B	10	5:01:34.9863	-4:15:55.874	−13.08	0.34	0.47	248
B	11	5:01:35.2150	-4:15:51.974	−13.57	0.35	0.34	208
E	1	5:01:37.7058	-4:15:57.405	−13.47	0.40	0.04	299
E	2	5:01:37.5314	-4:15:56.715	−15.80	0.20	0.36	875
E	3	5:01:37.2887	-4:15:48.075	−12.89	0.36	−0.00	277
F	4	5:01:39.8016	-4:16:21.525	−15.11	0.83	−0.63	550
F	5	5:01:39.8598	-4:16:22.515	−13.60	0.38	−0.24	333
F	6	5:01:40.1947	-4:16:26.835	−14.27	0.67	−0.47	373
F	7	5:01:40.2589	-4:16:28.755	−12.48	0.36	−0.30	286
G	1	5:01:44.0455	-4:17:21.045	−14.68	0.31	0.41	252
G	2	5:01:43.9492	-4:17:20.985	−14.83	0.34	0.41	298
G	3	5:01:43.9212	-4:17:22.665	−13.89	0.45	−0.01	190
G	4	5:01:43.8610	-4:17:22.305	−13.86	0.37	−0.01	187
G	5	5:01:43.7687	-4:17:19.245	−13.98	0.36	0.21	214
G	6	5:01:43.7206	-4:17:19.485	−13.06	0.17	0.15	139
G	7	5:01:43.6685	-4:17:17.625	−15.05	0.63	−0.23	307
G	8	5:01:43.8289	-4:17:14.445	−15.30	0.38	0.17	407
G	9	5:01:43.9011	-4:17:14.085	−14.99	0.49	−0.00	357
G	10	5:01:43.9492	-4:17:15.105	−13.50	0.32	0.37	198
G	11	5:01:44.0816	-4:17:13.965	−13.58	0.26	0.20	184

TABLE 3
Ultraviolet Fluxes, Infrared Luminosities, and Star Formation Rates

UV+IR Region	*Swift* U	*Swift* $UVM2$	*Swift* $UVW1$	*Swift* $UVW2$	*GALEX* NUV	*GALEX* FUV	*Spitzer* L_{24}	SFR
			(10^{-14} erg s^{-1} cm^{-2} Å^{-1})				(log(erg s^{-1} Hz^{-1}))	($M_\odot$ yr^{-1})
A+C+E	2.1 ± 0.1	4.8 ± 0.2	3.0 ± 0.1	5.2 ± 0.2	4.3 ± 0.4	7.9 ± 0.8	30.29	8.11
B	0.34 ± 0.01	0.81 ± 0.03	0.46 ± 0.02	0.89 ± 0.04	0.77 ± 0.07	1.3 ± 0.1	28.84	0.78
F	0.25 ± 0.01	0.31 ± 0.01	0.31 ± 0.01	0.27 ± 0.02	0.16 ± 0.02	0.29 ± 0.03	28.06	0.19
G	0.56 ± 0.02	1.58 ± 0.05	0.82 ± 0.03	1.74 ± 0.08	1.5 ± 0.1	3.0 ± 0.3	29.21	1.47
Q	0.033 ± 0.001	0.079 ± 0.004	0.036 ± 0.002	0.088 ± 0.008	0.098 ± 0.009	0.17 ± 0.02	27.46	0.07
Total							30.34	10.62

FIG. 1.— A five-color composite image of HCG 31 composed of purple (NUV *GALEX*), blue (B_{435} *HST*), yellow-green (V_{606} *HST*), orange (8 μm *Spitzer*), and red (I_{814} *HST*) images; see § 2.8. Group galaxies and tidal debris are labeled in light gray; HCG 31D (the red spiral in the upper right) is in the background. Young, massive stars are evident in blue and purple, and dust emission shows up as light orange. In general, the brightest nebular emission regions glow pink, because they have both strong UV and dust emission. However, regions such as tidal feature F with less pronounced IR emission appear turquoise due to H_α emission falling within the wide V_{606}. The 30″ scale corresponds to roughly 8 kpc. North is up, and east is to the left.

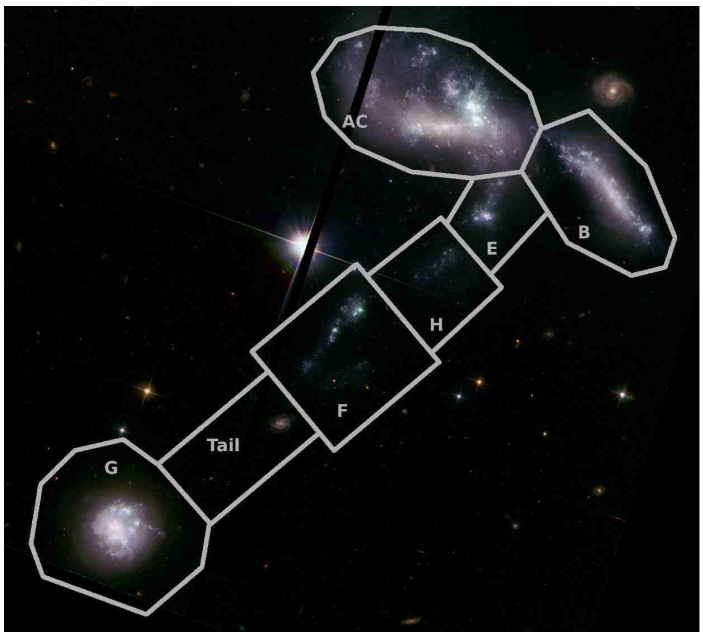

FIG. 2.— ACS three-color image of HCG 31. The gray polygons denote the boundaries of the physical regions associated with the galaxies and tidal structures in HCG 31 as labeled. They were defined by eye to encompass the optical light associated with each region.

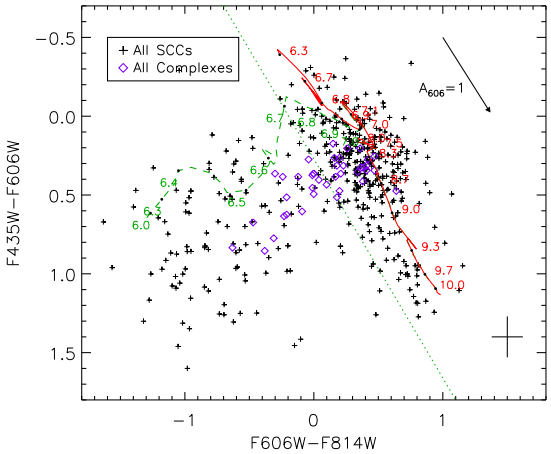

FIG. 3.— B_{435}–V_{606} vs. V_{606}–I_{814} color-color plots of the star cluster (SC) candidates (black crosses) with $M_{V_{606}} < -9$ and complexes (open purple diamonds) for the entire ACS field of view of HCG 31. The large black cross in the lower right corner indicates the median errors of the SC candidates; a Galactic reddening vector of A_{606}=1 is overplotted in the upper right corner. The solid, red curve is a Bruzual & Charlot (2003) evolutionary track for an instantaneous burst with 1/5 solar metallicity and a Salpeter initial mass function. The dashed green curve is an evolutionary track which includes nebular emission as described in section §2.5; the large numbers of SC candidates and complexes to the left of this track have colors indicating ages $\lesssim 5$ Myr. The positions of many of them below the dashed line is consistent with internal reddening shifting their colors. From visual inspection, most of the identified SC candidate and complexes have colors that are consistent with 10^7–10^8 yrs. For these sources, the tracks are almost parallel to the reddening vector, and there is considerable age-reddening degeneracy in this region of color space. Few globular cluster candidates are expected in this figure given the bright V_{606} luminosity limit.

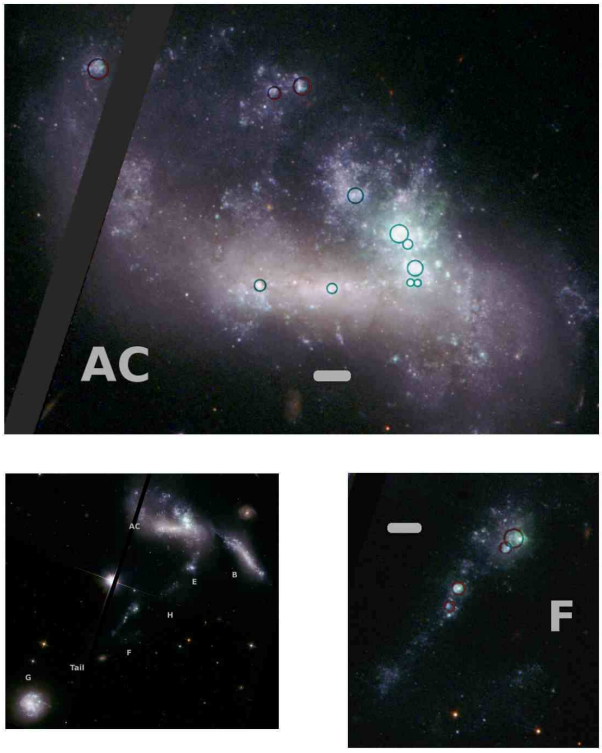

FIG. 4.— Star-forming complexes are shown in the three-color ACS images of HCG 31. The whole field is shown in the lower left, with the galaxies and tidal structures labeled. Close-ups of A+C and F are shown in subsequent frames. Measured complexes are indicated by solid circles with colors chosen to enhance visibility. Note that these complexes may encompass several star clusters. The thick, gray bar in each image represents 1 kpc.

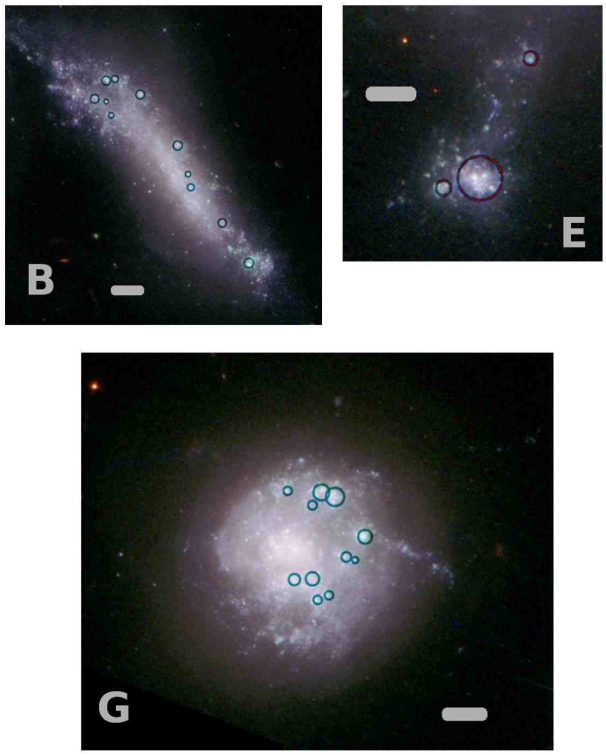

FIG. 5.— Same as Figure 4 for B, E, and G. The thick, gray bar in each image represents 1 kpc.

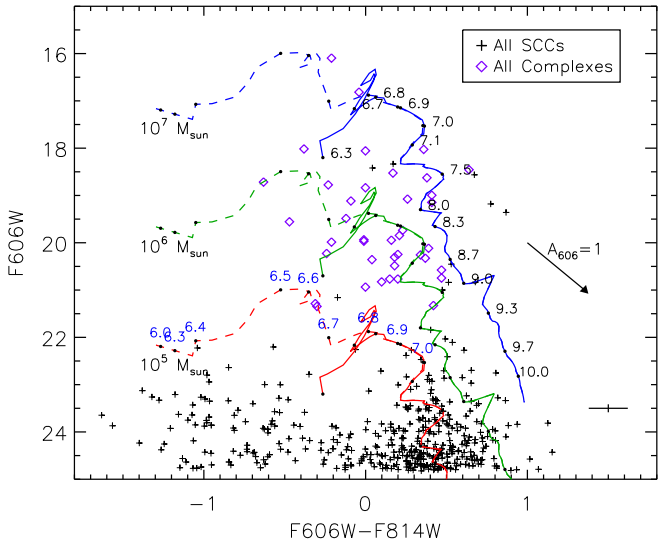

FIG. 6.— A V_{606} vs. V_{606}–I_{814} color-magnitude diagram for the SC candidates (black crosses) with $M_{V_{606}} < -9$ and complexes (open purple diamonds). The evolutionary tracks for 10^5, 10^6, and 10^7 $M_\odot$ clusters are indicated with the curves as labeled; dashed curves include nebular emission. Galactic extinction of $A_{606} = 1$ has been indicated with a labeled vector, and log(ages) in years are marked. The median color-magnitude error is indicated by the large black cross in the lower right corner. SC candidates consistent with having masses $> 10^6 M_\odot$ are found; the majority have V_{606}–I_{814} colors ranging from 0.2–0.6.

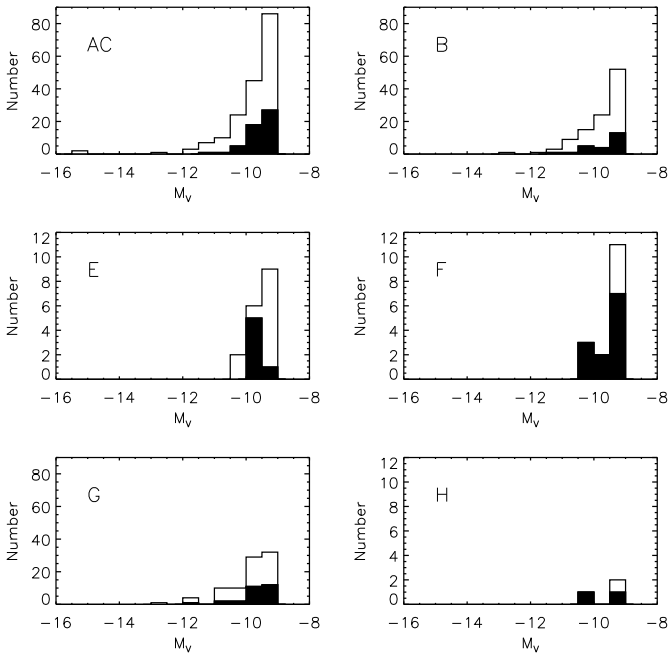

FIG. 7.— In each panel, the $M_{V_{606}}$ distributions of star cluster (SC) candidates with $M_{V_{606}} < -9$ for each region as labeled. Filled black histograms represent the distribution for SC candidates with nebular colors (see caption to Figure 3). The histograms overall are consistent with power-law distributions as found in other star-forming systems.

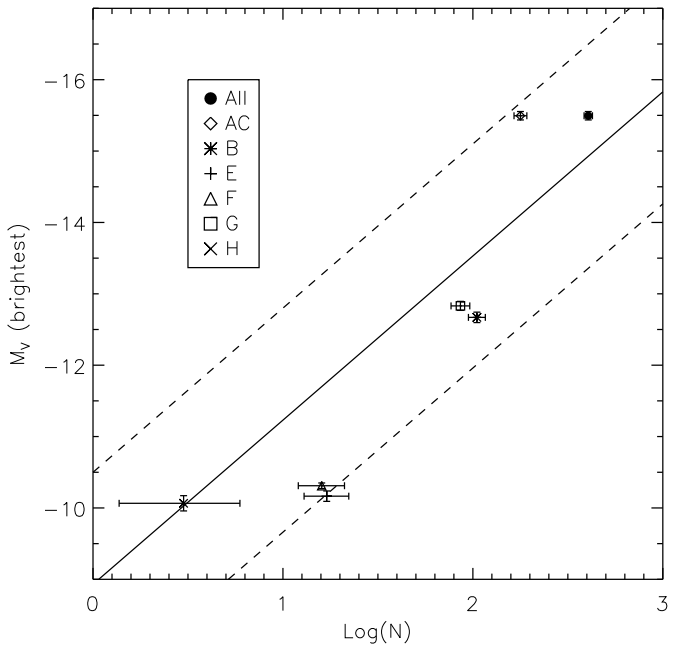

FIG. 8.— The absolute magnitude, $M_{V_{606}}$, of the brightest cluster in each region vs. $\log(N)$ (where N is the number of star cluster candidates brighter than $M_{V_{606}} = -9$ which excludes the majority of globular cluster candidates) for the entire ACS field. Each region is as labeled in the legend. Though no color criteria were applied to the selection of the brightest clusters, they are all young and blue. The errors in the ordinate are from poisson counting statistics, and the abscissa errors are photometric. The SC candidate populations in HCG 31 are consistent with the best-fitting linear fit (solid line) from the study of Whitmore et al. (2007) of 40 local star-forming galaxies, none of which were in compact groups. The scatter is also consistent; the dashed lines encompass 90% of their sample. Whitmore et al. (2007) interpret this correlation as a consequence of larger SC populations being statistically more likely to sample the bright end of the luminosity function.

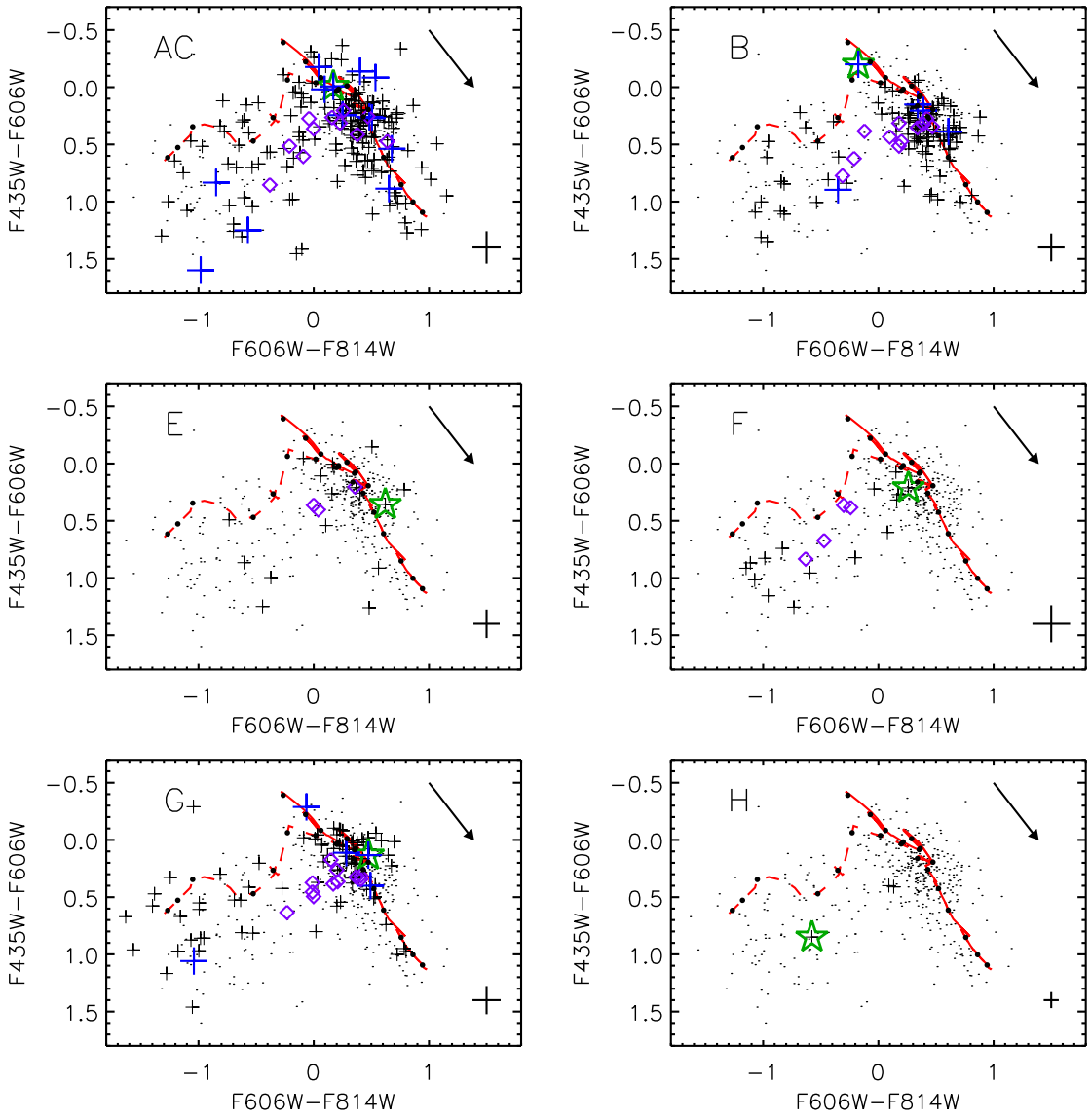

FIG. 9.— B_{435}–V_{606} vs. V_{606}–I_{814} color-color plots of the SC candidates with $M_{V_{606}} < -9$ and complexes in HCG 31. In each panel, black dots indicate all SC candidates from the entire ACS field of view, black crosses represent candidates within the region as labeled and shown in Figure 2. Larger, blue crosses are the more luminous ($M_{V_{606}} < -11$) SC candidates, the most luminous SC candidate is indicated with an open, green star, and open purple diamonds are the complexes. The large black cross in the lower right corner indicates the median color errors for the SC candidates in each region. Evolutionary tracks and reddening vectors are as described in the caption to Figure 3. The SC clusters are concentrated in the galaxies A+C, B, and G, though some are also found in the tidal features E, F, and H. Complexes are found in both galaxies and tidal features, with the exception of H. From comparison of the colors with the evolutionary tracks, all regions have SC candidates with ages $< 10^7$ yr and significant nebular emission, and only F and H show no evidence for SC candidates with ages $\gtrsim 500$ Myr.

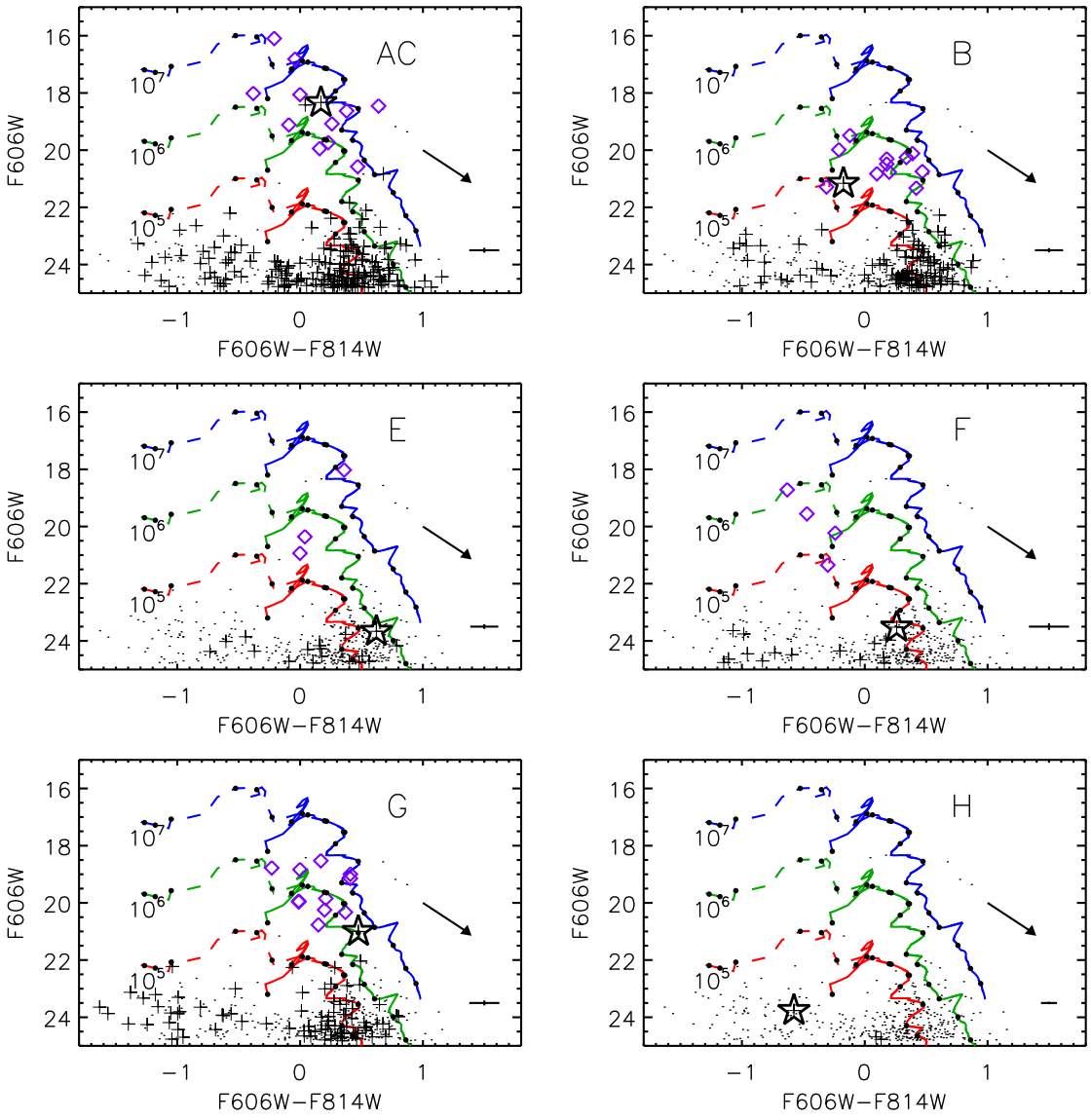

FIG. 10.— V_{606} vs. V_{606}–I_{814} color-magnitude plots of the SC candidates with $M_{V_{606}} < -9$ and complexes in HCG 31. In each panel, black dots indicate all SC candidates from the entire ACS field of view, black crosses represent candidates within the region as labeled and shown in Figure 2, the open black star is teh most luminous SC candidate, and open purple diamonds are the complexes. The median color-magnitude error in each region is shown with a large black cross in the lower right corner. Evolutionary tracks and reddening vectors are as described in the caption to Figure 6. By comparison with the evolutionary tracks, A+C has both complexes and SC candidates that are consistent with masses up to 10^{6-7}M$_\odot$, notably more massive than those in G and B. The tidal features E and F also host massive complexes, though their SC candidate populations are not as massive as those found in the galaxies A+C, B and G.

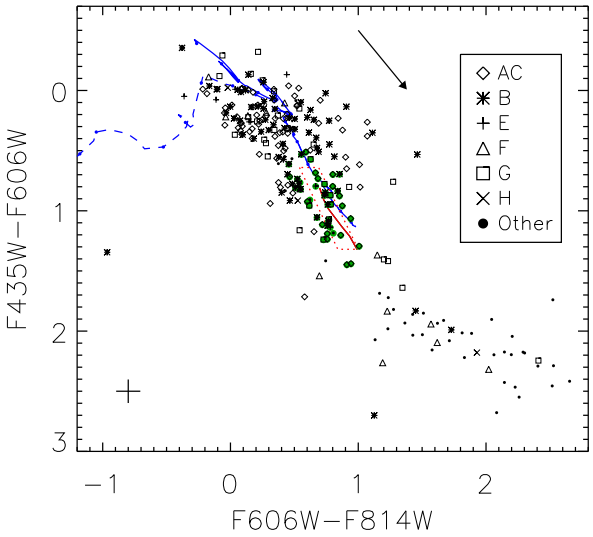

FIG. 11.— Color-color diagram for all point sources with $-13.8 < M_{V_{606}} < -7.8$ ($20 < V_{606} < 26$) where the strict point source selection criteria are defined in §2.1; this selection is designed to identify globular cluster candidates. The red dotted region denotes the expected colors for Milky Way globular clusters based on the Harris (1996) catalog; see §3.4 for details. The solid, red line within the detection region shows the predicted colors for old stellar populations from the simple stellar population models of Maraston (2005). Black symbols indicate the regions where the point sources are located (see legend for key); green circles underlie the 43 objects whose photometric error ellipses intersected the GC selection region. The median color-color errors are plotted as a large cross in the lower left corner. For reference, the nebular (blue, dashed) and normal (blue, solid) evolutionary tracks as described in §2.5 and an A_{606}=1 reddening vector are overplotted. Note the lack of strictly defined point sources with nebular colors compared to Figure 3; this shows that the vast majority of nebular sources are marginally resolved in the V_{606} image.

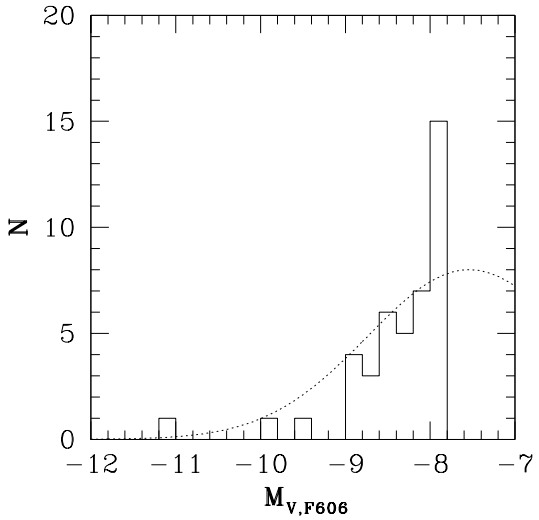

FIG. 12.— Raw V_{606} luminosity function (histogram) for all GC candidates with no correction made for any (small) background contamination or for photometric completeness. The dotted line shows the expected luminosity function for GCs located at the distance of HCG 31: a peak magnitude of $M_{V_{606}} = -7.4$ (corresponding to $V_{606} = 26.3$) and a dispersion of $\sigma = 1.2$. The plotted function is *not* a fit to the histogram, but is shown to indicate its expected shape.

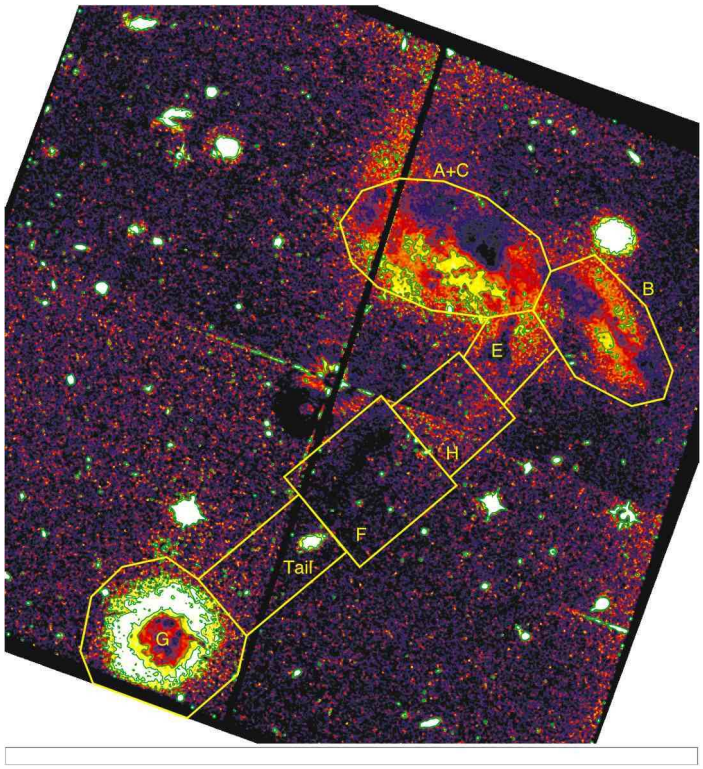

FIG. 13.— A Vega-magnitude calibrated, point-source subtracted, boxcar-smoothed (with a 13 pix window), B_{435}–I_{814} image of HCG 31. The image has been corrected for Galactic extinction. The scale is linear, and plotted colors range from −0.9 (black) to 1.9 (white). The blue-red transition occurs at B_{435}–I_{814}=0.4, and B_{435}–I_{814}=0.7 and 1.0 contours are plotted in green. Regions are labeled as in Figure 2. The lack of red in much of the F region indicates that there is no evidence for an older stellar population in the diffuse emission in that region. In contrast, the tidal material pulled out to the north of A+C and coincident with E and H clearly has redder colors (B_{435}–I_{814}=0.4–0.9).

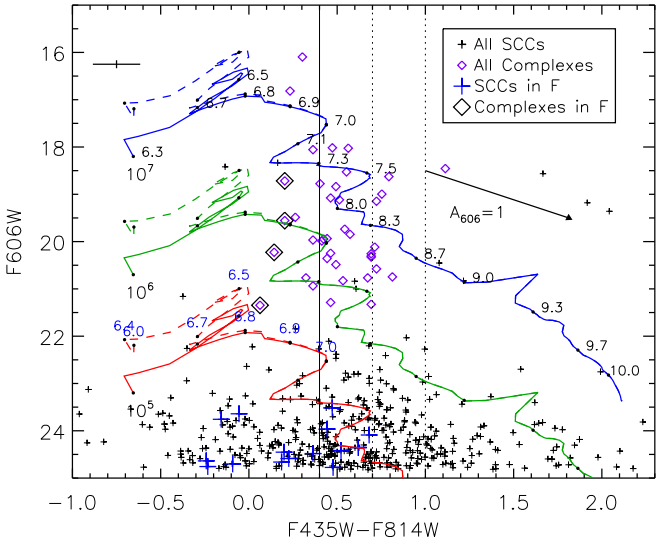

FIG. 14.— V_{606} vs. B_{435}–I_{814} color-magnitude diagram of the SC candidates and complexes; symbols and tracks are as described in the caption to Figure 6 with the addition of large crosses and diamonds to mark the objects in F. The vertical lines at B_{435}–I_{814}=0.4, 0.7, and 1.0 mark the blue-red transition and the green contour levels in the image shown in Figure 13. B_{435}–I_{814} color is not sensitive to nebular emission, and old (> 500 Myr) star clusters are expected to have B_{435}–$I_{814} \gtrsim 1.0$. From their colors, the SC candidates and complexes in F are notably young with B_{435}–I_{814} values extending from –0.3 to 0.7.